

A Benchmarking of QCD evolution at Approximate N³LO

A. Cooper-Sarkar^a, T. Cridge^b, F. Giuli^c, L. A. Harland-Lang^d, F. Hekhorn^{e,f}, J. Huston^g, G. Magni^{h,i}, S. Moch^j, R.S. Thorne^d

^a Department of Physics, University of Oxford, Oxford, OX1 3RH, UK

^b Deutsches Elektronen-Synchrotron DESY, Notkestr. 85, 22607 Hamburg, Germany

^c CERN, CH-1211 Geneva, Switzerland

^d Department of Physics and Astronomy, University College London, London, WC1E 6BT, UK

^e University of Jyväskylä, Department of Physics, P.O. Box 35, FI-40014 University of Jyväskylä, Finland

^f Helsinki Institute of Physics, P.O. Box 64, FI-00014 University of Helsinki, Finland

^g Department of Physics and Astronomy, Michigan State University, East Lansing, MI 48824, USA

^h Department of Physics and Astronomy, Vrije Universiteit, NL-1081 HV Amsterdam

ⁱ Nikhef Theory Group, Science Park 105, 1098 XG Amsterdam, The Netherlands

^j II. Institute for Theoretical Physics, Hamburg University, D-22761 Hamburg, Germany

Abstract

We present a detailed benchmarking of different treatments of the QCD evolution of unpolarized PDFs at approximate N³LO (aN³LO) order in the QCD coupling. Namely, the implementations in the public aN³LO releases of the MSHT and NNPDF global PDF fitters, as well as that of the theoretical FHMRUVV collaboration are compared. This follows the same procedure as in previous benchmarking exercises at lower orders, that is by considering the impact of this evolution on a set of simple toy PDFs. Excellent agreement between the MSHT and NNPDF results is found at NNLO, and at aN³LO when the same (FHMRUVV) implementation of the splitting functions is used. In addition, in the data region only small differences between these is seen when their original approximations are used for the splitting functions. The origin of these differences, and the larger ones observed at lower x , is well understood in terms of the differences in the approximate splitting functions. Good convergence is also observed between the exact and truncated solution methods for the DGLAP evolution equations. Overall, this provides confidence in the precision of the existing implementation of PDF evolution at N³LO.

1 Introduction

The scale dependence of parton distribution functions (PDFs) is governed by QCD evolution equations whose kernels, the splitting functions, are accessible within QCD perturbation theory. For about 20 years next-to-next-to-leading order (NNLO) has been the standard for precision predictions in perturbative QCD, including studies of the proton structure and fits of PDFs. For the solution of the integro-differential equations describing parton evolution in QCD, different codes have been developed within the community, making it necessary to check that there is consistency between the evolution codes used by the various groups. To this end a set of benchmark tables for parton evolution up to NNLO accuracy was produced in [1, 2] in order to provide a means of checking the (numerical) accuracy of any evolution code.

Given the increasing experimental precision and the challenge to push the accuracy of QCD perturbation theory by one quantum loop beyond the state-of-the-art, it is now necessary to extend the benchmarking of QCD evolution codes to the next order, i.e. next-to-NNLO (N³LO) in perturbative QCD. In this document, we provide a new set of benchmark tables for the evolution of unpolarized PDFs.¹ As the required QCD splitting functions are not yet fully known at this order, we resort to approximations which are valid within a restricted kinematic range. The outcomes of this study are

- benchmarking of available codes for parton evolution to N³LO.
- discussion and comparisons of different approximations for the QCD splitting functions at N³LO.

¹A short summary has been published as part of the activities of the “Standard Model” working group for the “Physics at TeV Colliders” workshop (Les Houches, France, 12–30 June, 2023) [3].

We provide a brief summary of the theoretical status of unpolarized parton evolution in QCD in Sec. 2, including a list of available tools and codes. We also discuss the different approximations for the N³LO splitting functions. The results and tables with benchmark numbers are listed in Sec. 3. We finish with conclusions and an outlook in Sec. 4.

2 Evolution equations and their solutions

2.1 The renormalization group equations

The scale evolution of the parton distributions $f_p(x, \mu_f^2) \equiv p(x, \mu_f^2)$, where $p = q_i, \bar{q}_i, g$ with $i = 1, \dots, n_f$, is governed by the $2n_f + 1$ coupled integro-differential equations

$$\frac{d f_p(x, \mu_f^2)}{d \ln \mu_f^2} = \sum_{l=0}^m a_s^{l+1}(\mu_r^2) \mathcal{P}_{pp'}^{(l)}\left(x, \frac{\mu_f^2}{\mu_r^2}\right) \otimes f_{p'}(x, \mu_f^2), \quad (1)$$

where summation over p' is understood. The factorization and renormalization scales are denoted μ_f and μ_r , and \otimes is the standard Mellin convolution in the fractional-momentum variable x . The scale dependence of the strong coupling reads

$$\frac{d a_s}{d \ln \mu_r^2} = \beta_{\text{N}^m\text{LO}}(a_s) = - \sum_{l=0}^m a_s^{l+2} \beta_l, \quad (2)$$

where we abbreviate $a_s \equiv \alpha_s/(4\pi)$. The β -function coefficients β_l are known to five loops in QCD [4, 5, 6, 7], which allows for the solution of Eq. (2) through N⁴LO for the a_s evolution.

The general splitting functions $\mathcal{P}^{(l)}$ in Eq. (1) reduce to the simpler expressions $P^{(l)}(x)$ at equal scales $\mu_r = \mu_f$. Up to N³LO the corresponding relations read

$$\begin{aligned} \mathcal{P}^{(0)}\left(x, \frac{\mu_f^2}{\mu_r^2}\right) &= P^{(0)}(x), \\ \mathcal{P}^{(1)}\left(x, \frac{\mu_f^2}{\mu_r^2}\right) &= P^{(1)}(x) - \beta_0 P^{(0)}(x) \ln \frac{\mu_f^2}{\mu_r^2}, \\ \mathcal{P}^{(2)}\left(x, \frac{\mu_f^2}{\mu_r^2}\right) &= P^{(2)}(x) - \left\{ \beta_1 P^{(0)}(x) + 2\beta_0 P^{(1)}(x) \right\} \ln \frac{\mu_f^2}{\mu_r^2} + \beta_0^2 P^{(0)}(x) \ln^2 \frac{\mu_f^2}{\mu_r^2}, \\ \mathcal{P}^{(3)}\left(x, \frac{\mu_f^2}{\mu_r^2}\right) &= P^{(3)}(x) - \left\{ \beta_2 P^{(0)}(x) + 2\beta_1 P^{(1)}(x) + 3\beta_0 P^{(2)}(x) \right\} \ln \frac{\mu_f^2}{\mu_r^2} \\ &\quad + \left\{ \frac{5}{2} \beta_0 \beta_1 P^{(0)}(x) + 3\beta_0^2 P^{(1)}(x) \right\} \ln^2 \frac{\mu_f^2}{\mu_r^2} - \beta_0^3 P^{(0)}(x) \ln^3 \frac{\mu_f^2}{\mu_r^2}. \end{aligned} \quad (3)$$

The splitting functions are currently known completely up to NNLO, i.e. analytic expression for $P_{pp'}^{(2)}(x)$ are available [8, 9]. At N³LO, this is also the case for non-singlet splitting functions in the planar limit [10] as well as for some parts of the functions $P_{pp'}^{(3)}(x)$ proportional to powers of n_f [11, 12, 13, 14]. In addition, there are a number of Mellin moments available for all splitting functions at N³LO [15, 16, 17, 18, 19, 20] (at least the first five moments, often ten or even more for specific colour factors). This information, taken together with knowledge on the functional form of the splitting functions in the limits $x \rightarrow 1$ and $x \rightarrow 0$, to be discussed below, serves as the basis for approximations to all N³LO splitting functions, allowing for a solution of Eq. (1) to this order.

2.2 Heavy-quark treatment

The renormalization group equations, Eqs. (1) and (2), are viable for a fixed number of flavors n_f and so we need to specify the prescription for changing n_f . The transition $n_f \rightarrow n_f + 1$ is made at the scales of the heavy-quark pole masses,

$$m_c = \sqrt{2} \text{ GeV}^2, \quad m_b = 4.5 \text{ GeV}^2. \quad (4)$$

The matching conditions for the strong coupling in the transition $n_f \rightarrow n_f + 1$ derive from the decoupling formulae, given by

$$a_s^{(n_f+1)}(k_r m_h^2) = a_s^{(n_f)}(k_r m_h^2) + \sum_{n=1}^m \left(a_s^{(n_f)}(k_r m_h^2) \right)^{n+1} \sum_{l=0}^n c_{n,l} \ln k_r. \quad (5)$$

The matching coefficients $c_{n,l}$ are known to four loops [21, 22], so that five-loop running can be obtained consistently from Eq. (2), taking into account threshold effects. The benchmark computations presented here use running $a_s^{(n_f)}$ at N³LO with the four-loop β -function.

The matching conditions at these thresholds $\mu_f^2 = m_h^2$, $h = c, b, t$ for the PDFs involve the operator matrix elements (OMEs) with heavy-quarks, $A_{pp'}(x)$, which are accessible in perturbation theory in an expansion in a_s with coefficients $A_{pp'}^{(l)}$, known [23] to two loops, i.e. $A_{pp'}^{(2)}$. For the benchmark computations, we apply these conditions up to NNLO(=N^{m=2}LO) and they read [24] ($\delta_{m2} = 1$ at N^{m=2}LO below)

$$l_i^{(n_f+1)}(x, m_h^2) = l_i^{(n_f)}(x, m_h^2) + \delta_{m2} a_s^2 A_{qq,h}^{NS,(2)}(x) \otimes l_i^{(n_f)}(x, m_h^2), \quad (6)$$

where $l = q, \bar{q}$ and $i = 1, \dots, n_f$, and

$$\begin{aligned} g^{(n_f+1)}(x, m_h^2) &= g^{(n_f)}(x, m_h^2) + \\ &\quad \delta_{m2} a_s^2 \left[A_{gq,h}^{S,(2)}(x) \otimes \Sigma^{(n_f)}(x, m_h^2) + A_{gg,h}^{S,(2)}(x) \otimes g^{(n_f)}(x, m_h^2) \right], \\ (h + \bar{h})^{(n_f+1)}(x, m_h^2) &= \delta_{m2} a_s^2 \left[\tilde{A}_{hq}^{S,(2)}(x) \otimes \Sigma^{(n_f)}(x, m_h^2) + \tilde{A}_{hg}^{S,(2)}(x) \otimes g^{(n_f)}(x, m_h^2) \right], \end{aligned} \quad (7)$$

where $h = \bar{h}$ and $\Sigma^{(n_f)} \equiv \sum_{i=1}^{n_f} (q_i + \bar{q}_i)$. The N³LO QCD corrections to massive OMEs are also available [25, 26, 27]. Those for $\tilde{A}_{hg}^{S,(3)}$ have recently been completed [28, 29], superseding previous approximations [30, 31].

The massive OMEs also provide the transition matrix elements in the variable-flavor number scheme (VFNS), where the transition $n_f \rightarrow n_f + 1$ treats one heavy-quark flavor at the time, i.e. the single-mass case [32]. At higher orders, both the c and b -quark loops appear in massive OMEs [33, 34, 35]. Accounting for those corrections requires the transition $n_f \rightarrow n_f + 2$, i.e. the two-mass case [36]. For the benchmark computations, the VFNS transition employs the single-mass case at NNLO only.

2.3 Available information and tools

As it is not possible to solve Eq. (1) in closed form beyond LO, a numerical algorithm has to be applied for which several public codes exist: APFEL [37], `apfel++` [38], EKO [39], HOPPET [40], PEGASUS [41], and QCDNUM [42]. The codes can be split into two different categories according to how they approach the solution of Eq. (1), by either taking a direct approach in momentum fraction space (APFEL, `apfel++`, HOPPET, QCDNUM) or solving in the conjugate Mellin-space (EKO, PEGASUS).

In the following we give a short review on the different approximation strategies applied by the MSHT group [43, 44], the NNPDF collaboration [45, 46], and FHMURVV [10, 17, 18, 19, 20] - for a detailed discussion we refer to the respective references.

2.3.1 MSHT

The first attempt to produce an approximate set of N³LO PDFs, incorporating the known information about the N³LO, i.e. $\mathcal{O}(\alpha_s^4)$, splitting functions was made by the MSHT group [43]. At the time this study took place less information was available than is currently the case. The approximation for the splitting functions was based on the following procedure (precise details can be found in [43]).

- Information on the Mellin moments of the splitting functions [10, 16] was used.
- The full information on the non-singlet splitting function presented in [10] was used. This includes information at high x from [47] as well as information appropriate in the limit of large flavour and colour number.

- The available information on leading $\ln(1/x)$ resummations from [48, 49, 50, 51, 52, 53, 54, 55] was used.

For each splitting function the terms which are known exactly were input, together with a set of basis functions chosen to be concentrated over a variety of x regions. For each splitting function one more function than there are known Mellin moments was chosen (i.e. a set of 5 basis functions to accompany the 4 moments known at the time for singlet splitting functions and a set of 9 basis functions to accompany the 8 moments for the nonsinglet splitting function). This leaves an unknown parameter, ρ which reflects the splitting function uncertainty and was chosen to be the coefficient of the most divergent unknown piece of our set of basis functions at small x . The variation in this parameter was then constrained by two requirements: for allowed ρ at high x , when the other coefficients of basis parameters are determined by matching the full splitting functions to the known Mellin moments, then the splitting function corrections at N³LO should not be large compare to those at lower orders; at sufficiently small x , for a fixed value of ρ , the splitting function is required to be contained within the range of variation predicted from exploring a full range of choice of basis functions. Once a particular choice of basis functions has been made there is then a preferred value of ρ and a variation which incurs a χ^2 penalty, i.e. there is a prior based on all the available knowledge about the function and lower orders. This prior was then modified in a fit to data and a posterior “best-fit” value and uncertainty was obtained for the value of ρ for each splitting function. The constraints on the splitting functions were applied in moment space in order to determine the values of ρ , but the splitting function was then expressed in x space and evolution performed via numerical solution of the renormalization group equations in Eq. (1).

This approach was used in both the first release of the approximate N³LO PDFs [43] and subsequent work including also QED evolution [44], examining various aspects of the data used for the high x gluon in the aN³LO PDFs [56], and the first determination of the strong coupling at aN³LO in a global PDF fit [57].

2.3.2 NNPDF

The default program adopted by the NNPDF collaboration for DGLAP evolution is the recently published code EKO [39]. It focuses on solving Eq. (1) in terms of evolution kernel operators (EKOs) E which are independent from the actual PDF $f_p(x, \mu_f^2)$, depending only on the theory setup (such as perturbative orders or the initial scale $\mu_{f,0}^2$):

$$f_p(\mu_f^2) = E_{pp'}(\mu_f^2 \leftarrow \mu_{f,0}^2) \otimes f_{p'}(\mu_{f,0}^2) \quad (8)$$

The EKOs are computed in Mellin space and transformed to momentum fraction space via interpolation techniques. EKO provides several strategies for solving the respective renormalization group equations which are perturbatively equivalent, but differ by the number of resummed terms. As EKOs are independent of the boundary PDF values, they are ideally suited for a PDF fit and as such EKO is integrated into the `pipeline` framework [58].

The EKO strategy for approximating the N³LO splitting function $P^{(3)}$, can be summarized as follows:

- The available information from soft gluon resummation in the threshold region $x \rightarrow 1$ [10, 11, 47, 59, 60, 61] is used.
- The available information from BFKL resummation in the high-energy region $x \rightarrow 0$ [48, 49, 50, 51, 52, 53, 62, 63, 64] is used.
- The available information in the limit of large number of flavors [10, 11, 12, 14] is used.
- The available information on the low Mellin moments [10, 16, 17, 18, 19] is used.

All limits are combined in a unique way and a number of sub-leading terms corresponding to the number of known Mellin moments are added. Precise details can be found in Section 2 of [46]. In particular the specific choice of the form of the sub-leading terms is arbitrary and drawn from a pre-defined list. This freedom represents the uncertainty associated with the partial knowledge on splitting functions and is referred to as Incomplete Higher Order Uncertainty (IHOU). IHOU are estimated independently from other possible sources of theory errors, such as the incomplete perturbative expansion (referred to as missing higher order uncertainty (MHO)) [65, 66].

2.3.3 FHMRUVV

Approximate results for the N³LO splitting functions have been constructed based on the available Mellin moments [15, 16, 17, 18, 19, 20] and all known results for the large- x and small- x limits. The large- x behavior of the $\overline{\text{MS}}$ -scheme diagonal splitting functions reads

$$P_{pp, x \rightarrow 1}^{(l-1)}(x) = \frac{A_p^{(l)}}{(1-x)_+} + B_p^{(l)} \delta(1-x) + C_p^{(l)} \ln(1-x) - A_p^{(l)} + D_p^{(l)}, \quad (9)$$

where the four-loop cusp anomalous dimensions $A_p^{(4)}$ [59, 67] as well as the coefficients $C_p^{(4)}$ and $D_p^{(4)}$ [19, 47] are known analytically, while the virtual anomalous dimensions $B_p^{(4)}$ multiplying $\delta(1-x)$ have been determined in approximate form [68, 69]. For all N³LO splitting functions further large- x constraints are known [61, 70, 71] and are also used. Information on their small- x behavior is also available. In case of $P_{gg}^{(3)}$ it is governed by the BFKL logarithms, of which the next-to-leading logarithmic (NLL) correction has been calculated [52, 54] and transformed to the $\overline{\text{MS}}$ -scheme some time ago [72, 73] (for $P_{gq}^{(3)}$, see [55]). Sub-dominant small- x terms for all splitting functions have also been derived [62].

The procedure is then based on a total of 80 approximations featuring slightly different functional forms for the splitting functions $P_{pp'}^{(3)}(x)$, consistent with their respective known endpoint behaviour. These approximations define a range and for the two boundaries of this range selected representatives $P_{pp'A}^{(3)}(x)$ and $P_{pp'B}^{(3)}(x)$ are presented to provide the error bands for $n_f = 3, 4, 5$ light flavours. The quality of this procedure is tested through approximations of the known NNLO splitting functions, demonstrating good convergence and providing information on the range of x for which residual uncertainties due to missing higher Mellin moments are small.

The approximate N³LO splitting functions are valid at large- x , with the uncertainties increasing towards smaller values of x . The FHMRUVV results [10, 17, 18, 19] for $P_{qq}^{(3)}(x)$ (non-singlet and pure-singlet) and $P_{gg}^{(3)}(x)$, based on ten Mellin moments $N \leq 20$, are reliable approximations down to $x \simeq 10^{-4}$. The quantities $P_{gq}^{(3)}(x)$ and $P_{qq}^{(3)}(x)$, based on five Mellin moments $N \leq 10$, are reasonable approximations down to $x \simeq 10^{-3}$. Their convolution with PDFs will dampen the uncertainty at small- x , so that one gains one additional order of magnitude on the right hand side of the evolution in Eq. (1) due to fast falling PDFs as $x \rightarrow 1$. The N³LO approximations to splitting functions convoluted with PDFs are, therefore, reliable in the range $10^{-5} \lesssim x \leq 1$ ($P_{qq}^{(3)}(x)$, $P_{gq}^{(3)}(x)$) and $10^{-4} \lesssim x \leq 1$ ($P_{gg}^{(3)}(x)$, $P_{qq}^{(3)}(x)$), respectively. The latest results for $P_{gq}^{(3)}(x)$ [20], based on ten Mellin moments ($N \leq 20$), have not been used in this benchmark comparison.

3 Benchmark tables

The corresponding lower order benchmark results are available at LO and NLO in [1] and at NNLO in [2], where LO and NLO polarized evolution has also been included. A number of minor typos have been reported in [39, 74] and are listed here for completeness:

- In [1], table headers, the combination L_+ has to be defined as $L_+ = 2(\bar{d} + \bar{u})$.
- In [1], header of Tab. 1 $\alpha_s(\mu_f^2 = 10^4 \text{ GeV}^2) = 0.117574$, as pointed out in [2].
- In [1], Tab. 1, $xs_+(x = 0.5, \mu_f = 10^4 \text{ GeV}^2) = 7.3137 \cdot 10^{-4}$ for $n_f = 4$, and $xb_+(x = 10^{-7}, \mu_f = 10^4 \text{ GeV}^2) = 4.6071 \cdot 10^{+1}$ for $n_f = 3 \dots 5$, differ in the last digit.
- In [1], Tab. 4, the value $xu_v(x = 0.7, \mu_f = 10^4 \text{ GeV}^2) = 2.0102 \cdot 10^{-2}$, differs in the last digit.
- In [1], Tab. 3, the values $xL_-(x = 10^{-5}, \mu_f = 10^4 \text{ GeV}^2) = 1.0121 \cdot 10^{-4}$ and $xL_-(x = 10^{-1}, \mu_f = 10^4 \text{ GeV}^2) = 9.8435 \cdot 10^{-3}$, contain wrong exponents.
- In [2], Tab. 15, the values $xd_v(x = 10^{-7}, \mu_f = 10^4 \text{ GeV}^2) = 1.0699 \cdot 10^{-4}$ and $xg(x = 10^{-7}, \mu_f = 10^4 \text{ GeV}^2) = 9.9694 \cdot 10^2$, contain wrong exponents.

3.1 Initial conditions

The initial conditions for the reference results are taken from [1, 2] with the evolution starting at

$$\mu_{f,0}^2 = 2 \text{ GeV}^2, \quad (10)$$

and the parametrizations of input distributions are chosen as

$$\begin{aligned} xu_v(x, \mu_{f,0}^2) &= 5.107200 x^{0.8} (1-x)^3, \\ xd_v(x, \mu_{f,0}^2) &= 3.064320 x^{0.8} (1-x)^4, \\ xg(x, \mu_{f,0}^2) &= 1.700000 x^{-0.1} (1-x)^5, \\ x\bar{d}(x, \mu_{f,0}^2) &= 0.1939875 x^{-0.1} (1-x)^6, \\ x\bar{u}(x, \mu_{f,0}^2) &= (1-x) x\bar{d}(x, \mu_{f,0}^2), \\ xs(x, \mu_{f,0}^2) &= x\bar{s}(x, \mu_{f,0}^2) = 0.2x(\bar{u} + \bar{d})(x, \mu_{f,0}^2), \end{aligned} \quad (11)$$

where the valence distributions are defined as $q_{i,v} \equiv q_i - \bar{q}_i$ and the value for the running coupling at the input scale is fixed as

$$\alpha_s(\mu_r^2 = 2 \text{ GeV}^2) = 0.35. \quad (12)$$

These initial conditions are used regardless of the perturbative order of the evolution and of the ratio of the renormalization and factorization scales, which take the values

$$\mu_r^2 = k_r \mu_f^2, \quad k_r = 0.5, 1, 2, \quad (13)$$

except for LO, where this ratio is fixed to unity.

We assume two different setups for the heavy quark treatment discussed in Section 2.2:

1. We assume a fixed number $n_f = 4$ of quarks participating in DGLAP evolution and we refer to this as the Fixed Flavor Number scheme (FFNS). We assume that all distributions in Eq. (11) are given directly in this scheme and that the charm distribution vanishes at the initial scale $\mu_{f,0}^2$. Similarly, we assume that the boundary condition of the strong coupling Eq. (12) is given in this scheme.
2. We assume a dynamic range $n_f = 3 \dots 5$ of participating quark flavors for our Variable Flavor Number scheme (VFNS), where each quark (here charm and bottom) gets activated when the evolution scale matches the quark mass. We assume Eqs. (11) and (12) apply for $n_f = 3$, such that an immediate matching procedure is triggered at the beginning of the evolution.

3.2 Results

The benchmark values are reported in the same basis adopted in [2], and we define:

$$q_v = q - \bar{q}, \quad L_- = (\bar{d} - \bar{u}), \quad L_+ = 2(\bar{d} + \bar{u}), \quad q_+ = q + \bar{q}. \quad (14)$$

In order to simplify the comparison, only NNLO matching conditions are adopted, although the N³LO coefficients are now available in literature and implemented in the evolution tools. The evolved PDFs are then evaluated at a final scale $\mu_f^2 = 10^4 \text{ GeV}^2$, which is chosen as representative for LHC processes. As a preliminary condition to the N³LO benchmark, we have tested that the different evolution codes are able to reproduce the NNLO benchmark tables of [2] with an accuracy of 0.01% or below. We adopt the same notation as in the previous study and write $x^a = x \times 10^a$.

In Tables 1 to 5 we report the central values for the FFNS aN³LO evolution for the 3 different splitting function approximations from FHMRUVV, MSHT and NNPDF respectively. The first part of the table refers to the central scale $\mu_f = \mu_r$ while the second and the third parts refer to the scale varied results. For MSHT we report only the values at the central scale $\mu_f = \mu_r$. Taking the same splitting function approximations from FHMRUVV as input, Tables 1 and 2 show a comparison of the two aN³LO evolution codes used by MSHT20 and NNPDF in the FFNS scheme at the central scale $\mu_f = \mu_r$. In the range $10^{-5} \lesssim x \lesssim 0.5$ there is generally very good agreement between the two evolution codes, with slightly larger

Table 1: Results for the FFNS aN³LO evolution for the initial conditions and the input parton distributions given in Sec. 3.1, with the FHMRUVV splitting functions approximation and the MSHT20aN3LO code.

FHMRUVV in MSHT20aN3LO $n_f = 4, \mu_f^2 = 10^4 \text{ GeV}^2$								
x	xu_v	xd_v	xL_-	xL_+	xs_v	xs_+	xc_+	xg
$\mu_r^2 = \mu_f^2$								
1.0 ⁻⁷	1.1073 ⁻⁴	5.3078 ⁻⁵	7.8440 ⁻⁶	1.4895 ⁺²	-2.7409 ⁻⁵	7.3405 ⁺¹	7.2681 ⁺¹	1.0858 ⁺³
1.0 ⁻⁶	5.7851 ⁻⁴	3.1908 ⁻⁴	3.0969 ⁻⁵	7.1890 ⁺¹	-4.2596 ⁻⁵	3.5094 ⁺¹	3.4520 ⁺¹	5.0367 ⁺²
1.0 ⁻⁵	2.9147 ⁻³	1.6974 ⁻³	1.2301 ⁻⁴	3.3841 ⁺¹	7.7558 ⁻⁶	1.6245 ⁺¹	1.5791 ⁺¹	2.2274 ⁺²
1.0 ⁻⁴	1.3657 ⁻²	8.0056 ⁻³	4.7181 ⁻⁴	1.5175 ⁺¹	2.3197 ⁻⁴	7.0536 ⁺⁰	6.6950 ⁺⁰	9.0183 ⁺¹
1.0 ⁻³	5.9557 ⁻²	3.4379 ⁻²	1.7184 ⁻³	6.2980 ⁺⁰	4.0044 ⁻⁴	2.7362 ⁺⁰	2.4588 ⁺⁰	3.1320 ⁺¹
1.0 ⁻²	2.3118 ⁻¹	1.2953 ⁻¹	5.7449 ⁻³	2.2665 ⁺⁰	-2.3112 ⁻⁴	8.5192 ⁻¹	6.6316 ⁻¹	8.1503 ⁺⁰
1.0 ⁻¹	5.5109 ⁻¹	2.7129 ⁻¹	1.0031 ⁻²	3.9000 ⁻¹	-3.2796 ⁻⁴	1.1381 ⁻¹	5.9754 ⁻²	9.0578 ⁻¹
3.0 ⁻¹	3.5031 ⁻¹	1.3010 ⁻¹	2.9715 ⁻³	3.5600 ⁻²	-3.8277 ⁻⁵	9.0840 ⁻³	3.3480 ⁻³	8.4418 ⁻²
5.0 ⁻¹	1.2107 ⁻¹	3.1503 ⁻²	3.6016 ⁻⁴	2.4562 ⁻³	-3.2055 ⁻⁶	5.8459 ⁻⁴	1.7823 ⁻⁴	8.1560 ⁻³
7.0 ⁻¹	2.0068 ⁻²	3.0873 ⁻³	1.0076 ⁻⁵	6.3848 ⁻⁵	-1.1067 ⁻⁷	1.3107 ⁻⁵	3.9940 ⁻⁶	3.9250 ⁻⁴
9.0 ⁻¹	3.5111 ⁻⁴	1.7834 ⁻⁵	-5.9504 ⁻⁸	1.7816 ⁻⁷	-1.3937 ⁻¹⁰	6.9228 ⁻⁹	8.6110 ⁻⁹	1.2313 ⁻⁶

deviations observed in regions of x where PDFs are becoming very small, i.e., in the limits $x \rightarrow 0$ (vanishing valence PDFs) and $x \rightarrow 1$. This very good agreement among the evolution codes provides the basis for quantifying the aN³LO FFNS evolution, now with the splitting function approximations from MSHT20 as input (Table 3 with MSHT20 prior and Table 4 with MSHT20 posterior) using the MSHT20 code, and for the NNPDF approximations (Table 5) with the NNPDF code, cf. Section 2.3 for details. Due to the different methodology in preparing those approximations, larger deviations are observed as a result of the aN³LO evolution, especially for smaller x values, e.g., for the gluon PDF at $x \lesssim 10^{-3}$, when sufficient constraints on the splitting function $P_{gg}^{(3)}(x)$ from Mellin moments are lacking. In essence, these deviations demonstrate the current uncertainties inherent in the knowledge of the evolution kernels. However, these deviations would reduce with the use of more up to date input information for each of the groups determination of the splitting functions (particularly for the older MSHT determination).

The corresponding values for the VFNS evolution are listed in Tables 6 to 10. Tables 6 and 7 show again very good agreement in the same x range as before between the two aN³LO evolution codes (MSHT20 and NNPDF) with the FHMRUVV splitting function approximations, now employing the VFNS scheme, while Tables 8 and 9 (MSHT20 prior and posterior with the MSHT20 code) and Table 5 (NNPDF approximations with NNPDF code) in the VFNS scheme display the same similarities and differences as observed in the FFNS scheme.

For simplicity we only give the central values in Tables 1 to 10, while the complete set containing all evolved PDFs with all the splitting functions variations are available under the following URL:

<https://www.hep.ucl.ac.uk/pdf4lhc/aN3LObenchmarking.shtml>

The benchmark numbers are illustrated in Figs. 1 to 4, where we show the absolute and relative difference with respect to the NNLO evolution for the different aN³LO evolutions, for each PDF flavor combination, reported in the previous tables. We display the FFNS and VFNS settings respectively with the central scale $\mu_r = \mu_f$. The figures include an estimate of the uncertainties due to the approximated splitting functions, which is obtained by varying a single splitting function at a time during the evolution, and taking the uncertainty, for each point in x , as 1/2 of the spread of the final PDF. The displayed FHMRUVV result is averaged between the values obtained with the MSHT20 and NNPDF evolution codes. Since MSHT and NNPDF parametrizations do not include uncertainties for the non-singlet combinations, errors for the combinations d_v, u_v, s_v and L_- have been set to 0, though the difference from different approximations

Table 2: Results for the FFNS aN³LO evolution for the initial conditions and the input parton distributions given in Sec. 3.1, with the FHMRUVV splitting functions approximation and the NNPDF code.

FHMRUVV in NNPDF $n_f = 4, \mu_f^2 = 10^4 \text{ GeV}^2$								
x	xu_v	xd_v	xL_-	xL_+	xs_v	xs_+	xc_+	xg
$\mu_r^2 = \mu_f^2$								
1.0 ⁻⁷	9.8369 ⁻⁵	4.5170 ⁻⁵	7.5011 ⁻⁶	1.4885 ⁺²	-2.9106 ⁻⁵	7.3353 ⁺¹	7.2639 ⁺¹	1.0846 ⁺³
1.0 ⁻⁶	5.6405 ⁻⁴	3.0895 ⁻⁴	3.0730 ⁻⁵	7.1894 ⁺¹	-4.6738 ⁻⁵	3.5096 ⁺¹	3.4528 ⁺¹	5.0358 ⁺²
1.0 ⁻⁵	2.8946 ⁻³	1.6810 ⁻³	1.2302 ⁻⁴	3.3858 ⁺¹	-3.5753 ⁻⁶	1.6253 ⁺¹	1.5803 ⁺¹	2.2282 ⁺²
1.0 ⁻⁴	1.3633 ⁻²	7.9832 ⁻³	4.7274 ⁻⁴	1.5182 ⁺¹	2.1123 ⁻⁴	7.0571 ⁺⁰	6.7005 ⁺⁰	9.0222 ⁺¹
1.0 ⁻³	5.9567 ⁻²	3.4382 ⁻²	1.7231 ⁻³	6.3007 ⁺⁰	3.9314 ⁻⁴	2.7376 ⁺⁰	2.4611 ⁺⁰	3.1336 ⁺¹
1.0 ⁻²	2.3130 ⁻¹	1.2962 ⁻¹	5.7645 ⁻³	2.2668 ⁺⁰	-1.9644 ⁻⁴	8.5223 ⁻¹	6.6372 ⁻¹	8.1534 ⁺⁰
1.0 ⁻¹	5.5131 ⁻¹	2.7140 ⁻¹	1.0085 ⁻²	3.8981 ⁻¹	-3.1812 ⁻⁴	1.1389 ⁻¹	5.9850 ⁻²	9.0623 ⁻¹
3.0 ⁻¹	3.5044 ⁻¹	1.3015 ⁻¹	3.0144 ⁻³	3.5450 ⁻²	-3.8409 ⁻⁵	9.1019 ⁻³	3.3625 ⁻³	8.4444 ⁻²
5.0 ⁻¹	1.2112 ⁻¹	3.1518 ⁻²	3.7781 ⁻⁴	2.4085 ⁻³	-3.3051 ⁻⁶	5.9065 ⁻⁴	1.8276 ⁻⁴	8.1586 ⁻³
7.0 ⁻¹	2.0077 ⁻²	3.0900 ⁻³	1.3437 ⁻⁵	5.6818 ⁻⁵	-1.1797 ⁻⁷	1.4269 ⁻⁵	4.9009 ⁻⁶	3.9235 ⁻⁴
9.0 ⁻¹	3.4849 ⁻⁴	1.8135 ⁻⁵	1.3838 ⁻⁸	1.0982 ⁻⁷	-2.1740 ⁻¹⁰	4.2627 ⁻⁸	3.4628 ⁻⁸	1.3275 ⁻⁶
$\mu_r^2 = 2 \mu_f^2$								
1.0 ⁻⁷	1.1400 ⁻⁴	6.3301 ⁻⁵	6.5066 ⁻⁶	1.4118 ⁺²	-7.8056 ⁻⁶	6.9517 ⁺¹	6.8801 ⁺¹	1.0533 ⁺³
1.0 ⁻⁶	5.9327 ⁻⁴	3.4617 ⁻⁴	2.7505 ⁻⁵	6.9885 ⁺¹	6.1035 ⁻⁷	3.4090 ⁺¹	3.3522 ⁺¹	4.9859 ⁺²
1.0 ⁻⁵	2.9066 ⁻³	1.7186 ⁻³	1.1268 ⁻⁴	3.3325 ⁺¹	6.6447 ⁻⁵	1.5986 ⁺¹	1.5535 ⁺¹	2.2228 ⁺²
1.0 ⁻⁴	1.3478 ⁻²	7.9084 ⁻³	4.4131 ⁻⁴	1.5014 ⁺¹	2.3633 ⁻⁴	6.9723 ⁺⁰	6.6151 ⁺⁰	9.0028 ⁺¹
1.0 ⁻³	5.8973 ⁻²	3.4010 ⁻²	1.6441 ⁻³	6.2494 ⁺⁰	2.7889 ⁻⁴	2.7109 ⁺⁰	2.4339 ⁺⁰	3.1216 ⁺¹
1.0 ⁻²	2.3048 ⁻¹	1.2918 ⁻¹	5.6473 ⁻³	2.2597 ⁺⁰	-2.8956 ⁻⁴	8.4756 ⁻¹	6.5859 ⁻¹	8.1296 ⁺⁰
1.0 ⁻¹	5.5246 ⁻¹	2.7213 ⁻¹	1.0081 ⁻²	3.9105 ⁻¹	-2.8317 ⁻⁴	1.1407 ⁻¹	5.9775 ⁻²	9.0774 ⁻¹
3.0 ⁻¹	3.5229 ⁻¹	1.3092 ⁻¹	3.0315 ⁻³	3.5676 ⁻²	-3.2738 ⁻⁵	9.1494 ⁻³	3.3664 ⁻³	8.4779 ⁻²
5.0 ⁻¹	1.2205 ⁻¹	3.1785 ⁻²	3.8118 ⁻⁴	2.4251 ⁻³	-2.8167 ⁻⁶	5.9294 ⁻⁴	1.8094 ⁻⁴	8.2004 ⁻³
7.0 ⁻¹	2.0291 ⁻²	3.1256 ⁻³	1.3604 ⁻⁵	5.6613 ⁻⁵	-1.0201 ⁻⁷	1.3991 ⁻⁵	4.5001 ⁻⁶	3.9492 ⁻⁴
9.0 ⁻¹	3.5422 ⁻⁴	1.8440 ⁻⁵	1.4099 ⁻⁸	9.3900 ⁻⁸	-1.9148 ⁻¹⁰	3.4475 ⁻⁸	2.6320 ⁻⁸	1.3407 ⁻⁶
$\mu_r^2 = 0.5 \mu_f^2$								
1.0 ⁻⁷	4.4192 ⁻⁵	-1.1184 ⁻⁵	9.0493 ⁻⁶	1.6657 ⁺²	-8.7990 ⁻⁵	8.2215 ⁺¹	8.1501 ⁺¹	1.1828 ⁺³
1.0 ⁻⁶	4.3474 ⁻⁴	1.7517 ⁻⁴	3.5176 ⁻⁵	7.5683 ⁺¹	-1.8556 ⁻⁴	3.6992 ⁺¹	3.6425 ⁺¹	5.2150 ⁺²
1.0 ⁻⁵	2.6807 ⁻³	1.4586 ⁻³	1.3589 ⁻⁴	3.4392 ⁺¹	-2.3604 ⁻⁴	1.6521 ⁺¹	1.6071 ⁺¹	2.2470 ⁺²
1.0 ⁻⁴	1.3512 ⁻²	7.8398 ⁻³	5.1075 ⁻⁴	1.5206 ⁺¹	3.9416 ⁻⁵	7.0699 ⁺⁰	6.7139 ⁺⁰	9.0326 ⁺¹
1.0 ⁻³	5.9946 ⁻²	3.4688 ⁻²	1.8231 ⁻³	6.2896 ⁺⁰	6.1057 ⁻⁴	2.7333 ⁺⁰	2.4572 ⁺⁰	3.1414 ⁺¹
1.0 ⁻²	2.3195 ⁻¹	1.3013 ⁻¹	5.9287 ⁻³	2.2606 ⁺⁰	1.9683 ⁻⁴	8.5037 ⁻¹	6.6210 ⁻¹	8.1731 ⁺⁰
1.0 ⁻¹	5.5088 ⁻¹	2.7116 ⁻¹	1.0132 ⁻²	3.8936 ⁻¹	-3.0333 ⁻⁴	1.1393 ⁻¹	5.9982 ⁻²	9.0498 ⁻¹
3.0 ⁻¹	3.4987 ⁻¹	1.2993 ⁻¹	3.0140 ⁻³	3.5489 ⁻²	-4.1682 ⁻⁵	9.1433 ⁻³	3.4151 ⁻³	8.4372 ⁻²
5.0 ⁻¹	1.2088 ⁻¹	3.1453 ⁻²	3.7730 ⁻⁴	2.4190 ⁻³	-3.6076 ⁻⁶	5.9739 ⁻⁴	1.9043 ⁻⁴	8.1626 ⁻³
7.0 ⁻¹	2.0030 ⁻²	3.0824 ⁻³	1.3408 ⁻⁵	5.8137 ⁻⁵	-1.2487 ⁻⁷	1.4967 ⁻⁵	5.6241 ⁻⁶	3.9298 ⁻⁴
9.0 ⁻¹	3.4739 ⁻⁴	1.8076 ⁻⁵	1.3770 ⁻⁸	1.3969 ⁻⁷	-2.2060 ⁻¹⁰	5.7582 ⁻⁸	4.9611 ⁻⁸	1.3299 ⁻⁶

Table 3: Results for the FFNS aN³LO evolution for the initial conditions and the input parton distributions given in Sec. 3.1, with the MSHT20aN3LO prior splitting functions approximation.

MSHT20aN3LO prior $n_f = 4, \mu_f^2 = 10^4 \text{ GeV}^2$								
x	xu_v	xd_v	xL_-	xL_+	xs_v	xs_+	xc_+	xg
$\mu_r^2 = \mu_f^2$								
1.0 ⁻⁷	1.2189 ⁻⁴	6.7096 ⁻⁵	2.4727 ⁻⁶	5.2287 ⁺¹	-9.9201 ⁻⁶	2.5070 ⁺¹	2.4349 ⁺¹	4.0508 ⁺²
1.0 ⁻⁶	5.8593 ⁻⁴	3.3362 ⁻⁴	1.2769 ⁻⁵	3.4289 ⁺¹	-1.9932 ⁻⁵	1.6292 ⁺¹	1.5721 ⁺¹	2.6377 ⁺²
1.0 ⁻⁵	2.8965 ⁻³	1.6914 ⁻³	6.8967 ⁻⁵	2.1730 ⁺¹	1.3958 ⁻⁵	1.0188 ⁺¹	9.7359 ⁺⁰	1.5546 ⁺²
1.0 ⁻⁴	1.3619 ⁻²	7.9736 ⁻³	3.4675 ⁻⁴	1.2464 ⁺¹	2.0204 ⁻⁴	5.6972 ⁺⁰	5.3396 ⁺⁰	7.7766 ⁺¹
1.0 ⁻³	5.9587 ⁻²	3.4383 ⁻²	1.5513 ⁻³	6.1230 ⁺⁰	3.7152 ⁻⁴	2.6481 ⁺⁰	2.3710 ⁺⁰	3.0816 ⁺¹
1.0 ⁻²	2.3129 ⁻¹	1.2959 ⁻¹	5.7459 ⁻³	2.3265 ⁺⁰	-2.3233 ⁻⁴	8.8203 ⁻¹	6.9326 ⁻¹	8.4107 ⁺⁰
1.0 ⁻¹	5.5130 ⁻¹	2.7140 ⁻¹	1.0091 ⁻²	3.8948 ⁻¹	-3.2809 ⁻⁴	1.1372 ⁻¹	5.9658 ⁻²	9.0604 ⁻¹
3.0 ⁻¹	3.5044 ⁻¹	1.3015 ⁻¹	3.0182 ⁻³	3.5400 ⁻²	-3.8291 ⁻⁵	9.0869 ⁻³	3.3463 ⁻³	8.4342 ⁻²
5.0 ⁻¹	1.2111 ⁻¹	3.1516 ⁻²	3.7949 ⁻⁴	2.3927 ⁻³	-3.2067 ⁻⁶	5.8587 ⁻⁴	1.7784 ⁻⁴	8.1760 ⁻³
7.0 ⁻¹	2.0075 ⁻²	3.0885 ⁻³	1.3847 ⁻⁵	5.3271 ⁻⁵	-1.1071 ⁻⁷	1.2962 ⁻⁵	3.5378 ⁻⁶	3.8989 ⁻⁴
9.0 ⁻¹	3.5125 ⁻⁴	1.7841 ⁻⁵	1.6416 ⁻⁸	8.6161 ⁻⁹	-1.3944 ⁻¹⁰	6.3097 ⁻⁹	2.0583 ⁻⁹	1.1858 ⁻⁶

Table 4: Results for the FFNS aN³LO evolution for the initial conditions and the input parton distributions given in Sec. 3.1, with the MSHT20aN3LO posterior splitting functions approximation.

MSHT20aN3LO posterior $n_f = 4, \mu_f^2 = 10^4 \text{ GeV}^2$								
x	xu_v	xd_v	xL_-	xL_+	xs_v	xs_+	xc_+	xg
$\mu_r^2 = \mu_f^2$								
1.0 ⁻⁷	1.2189 ⁻⁴	6.7096 ⁻⁵	2.4727 ⁻⁶	8.4227 ⁺¹	-9.9201 ⁻⁶	4.1040 ⁺¹	4.0322 ⁺¹	7.1749 ⁺²
1.0 ⁻⁶	5.8593 ⁻⁴	3.3362 ⁻⁴	1.2769 ⁻⁵	4.4674 ⁺¹	-1.9932 ⁻⁵	2.1485 ⁺¹	2.0915 ⁺¹	3.6931 ⁺²
1.0 ⁻⁵	2.8965 ⁻³	1.6914 ⁻³	6.8967 ⁻⁵	2.3876 ⁺¹	1.3958 ⁻⁵	1.1261 ⁺¹	1.0810 ⁺¹	1.8224 ⁺²
1.0 ⁻⁴	1.3619 ⁻²	7.9736 ⁻³	3.4675 ⁻⁴	1.2426 ⁺¹	2.0204 ⁻⁴	5.6784 ⁺⁰	5.3212 ⁺⁰	8.1561 ⁺¹
1.0 ⁻³	5.9587 ⁻²	3.4383 ⁻²	1.5513 ⁻³	5.9728 ⁺⁰	3.7152 ⁻⁴	2.5730 ⁺⁰	2.2960 ⁺⁰	3.0671 ⁺¹
1.0 ⁻²	2.3129 ⁻¹	1.2959 ⁻¹	5.7459 ⁻³	2.3273 ⁺⁰	-2.3233 ⁻⁴	8.8244 ⁻¹	6.9366 ⁻¹	8.3365 ⁺⁰
1.0 ⁻¹	5.5130 ⁻¹	2.7140 ⁻¹	1.0091 ⁻²	3.9002 ⁻¹	-3.2809 ⁻⁴	1.1399 ⁻¹	5.9926 ⁻²	9.0673 ⁻¹
3.0 ⁻¹	3.5044 ⁻¹	1.3015 ⁻¹	3.0182 ⁻³	3.5367 ⁻²	-3.8291 ⁻⁵	9.0707 ⁻³	3.3300 ⁻³	8.4315 ⁻²
5.0 ⁻¹	1.2111 ⁻¹	3.1516 ⁻²	3.7949 ⁻⁴	2.3999 ⁻³	-3.2067 ⁻⁶	5.8951 ⁻⁴	1.8148 ⁻⁴	8.1793 ⁻³
7.0 ⁻¹	2.0075 ⁻²	3.0885 ⁻³	1.3847 ⁻⁵	5.2544 ⁻⁵	-1.1071 ⁻⁷	1.2598 ⁻⁵	3.1752 ⁻⁶	3.8961 ⁻⁴
9.0 ⁻¹	3.5125 ⁻⁴	1.7841 ⁻⁵	1.6416 ⁻⁸	-1.9342 ⁻⁹	-1.3944 ⁻¹⁰	1.0345 ⁻⁹	-3.2071 ⁻⁹	1.1788 ⁻⁶

Table 5: Results for the FFNS aN³LO evolution for the initial conditions and the input parton distributions given in Sec. 3.1, with the NNPDF splitting functions approximation.

NNPDF $n_f = 4$, $\mu_f^2 = 10^4 \text{ GeV}^2$								
x	xu_v	xd_v	xL_-	xL_+	xs_v	xs_+	xc_+	xg
$\mu_r^2 = \mu_f^2$								
1.0 ⁻⁷	9.1711 ⁻⁵	4.1520 ⁻⁵	6.3455 ⁻⁶	1.3633 ⁺²	-2.9134 ⁻⁵	6.7094 ⁺¹	6.6379 ⁺¹	9.9074 ⁺²
1.0 ⁻⁶	5.4825 ⁻⁴	3.0047 ⁻⁴	2.8366 ⁻⁵	6.8193 ⁺¹	-4.6755 ⁻⁵	3.3245 ⁺¹	3.2678 ⁺¹	4.7660 ⁺²
1.0 ⁻⁵	2.8653 ⁻³	1.6659 ⁻³	1.1996 ⁻⁴	3.3061 ⁺¹	-3.5228 ⁻⁶	1.5855 ⁺¹	1.5404 ⁺¹	2.1712 ⁺²
1.0 ⁻⁴	1.3605 ⁻²	7.9705 ⁻³	4.7399 ⁻⁴	1.5100 ⁺¹	2.1129 ⁻⁴	7.0162 ⁺⁰	6.6596 ⁺⁰	8.9608 ⁺¹
1.0 ⁻³	5.9601 ⁻²	3.4403 ⁻²	1.7396 ⁻³	6.3082 ⁺⁰	3.9309 ⁻⁴	2.7415 ⁺⁰	2.4650 ⁺⁰	3.1379 ⁺¹
1.0 ⁻²	2.3135 ⁻¹	1.2964 ⁻¹	5.7805 ⁻³	2.2682 ⁺⁰	-1.9645 ⁻⁴	8.5296 ⁻¹	6.6444 ⁻¹	8.1650 ⁺⁰
1.0 ⁻¹	5.5130 ⁻¹	2.7140 ⁻¹	1.0084 ⁻²	3.8980 ⁻¹	-3.1812 ⁻⁴	1.1388 ⁻¹	5.9847 ⁻²	9.0618 ⁻¹
3.0 ⁻¹	3.5044 ⁻¹	1.3015 ⁻¹	3.0144 ⁻³	3.5451 ⁻²	-3.8409 ⁻⁵	9.1020 ⁻³	3.3626 ⁻³	8.4445 ⁻²
5.0 ⁻¹	1.2112 ⁻¹	3.1518 ⁻²	3.7782 ⁻⁴	2.4085 ⁻³	-3.3051 ⁻⁶	5.9064 ⁻⁴	1.8275 ⁻⁴	8.1587 ⁻³
7.0 ⁻¹	2.0077 ⁻²	3.0900 ⁻³	1.3438 ⁻⁵	5.6818 ⁻⁵	-1.1797 ⁻⁷	1.4269 ⁻⁵	4.9012 ⁻⁶	3.9230 ⁻⁴
9.0 ⁻¹	3.4849 ⁻⁴	1.8135 ⁻⁵	1.3877 ⁻⁸	1.0977 ⁻⁷	-2.1739 ⁻¹⁰	4.2631 ⁻⁸	3.4632 ⁻⁸	1.3315 ⁻⁶
$\mu_r^2 = 2 \mu_f^2$								
1.0 ⁻⁷	1.1006 ⁻⁴	6.1143 ⁻⁵	5.8224 ⁻⁶	1.3396 ⁺²	-7.8173 ⁻⁶	6.5905 ⁺¹	6.5189 ⁺¹	9.9727 ⁺²
1.0 ⁻⁶	5.8391 ⁻⁴	3.4115 ⁻⁴	2.6103 ⁻⁵	6.7757 ⁺¹	6.1119 ⁻⁷	3.3026 ⁺¹	3.2458 ⁺¹	4.8250 ⁺²
1.0 ⁻⁵	2.8891 ⁻³	1.7096 ⁻³	1.1086 ⁻⁴	3.2868 ⁺¹	6.6482 ⁻⁵	1.5757 ⁺¹	1.5306 ⁺¹	2.1888 ⁺²
1.0 ⁻⁴	1.3461 ⁻²	7.9008 ⁻³	4.4203 ⁻⁴	1.4967 ⁺¹	2.3636 ⁻⁴	6.9487 ⁺⁰	6.5916 ⁺⁰	8.9657 ⁺¹
1.0 ⁻³	5.8993 ⁻²	3.4022 ⁻²	1.6540 ⁻³	6.2537 ⁺⁰	2.7886 ⁻⁴	2.7131 ⁺⁰	2.4361 ⁺⁰	3.1241 ⁺¹
1.0 ⁻²	2.3051 ⁻¹	1.2919 ⁻¹	5.6569 ⁻³	2.2605 ⁺⁰	-2.8957 ⁻⁴	8.4798 ⁻¹	6.5901 ⁻¹	8.1366 ⁺⁰
1.0 ⁻¹	5.5246 ⁻¹	2.7213 ⁻¹	1.0080 ⁻²	3.9105 ⁻¹	-2.8317 ⁻⁴	1.1407 ⁻¹	5.9773 ⁻²	9.0772 ⁻¹
3.0 ⁻¹	3.5229 ⁻¹	1.3092 ⁻¹	3.0315 ⁻³	3.5676 ⁻²	-3.2738 ⁻⁵	9.1495 ⁻³	3.3665 ⁻³	8.4780 ⁻²
5.0 ⁻¹	1.2205 ⁻¹	3.1785 ⁻²	3.8118 ⁻⁴	2.4251 ⁻³	-2.8167 ⁻⁶	5.9293 ⁻⁴	1.8093 ⁻⁴	8.2005 ⁻³
7.0 ⁻¹	2.0291 ⁻²	3.1256 ⁻³	1.3604 ⁻⁵	5.6612 ⁻⁵	-1.0201 ⁻⁷	1.3991 ⁻⁵	4.5003 ⁻⁶	3.9489 ⁻⁴
9.0 ⁻¹	3.5422 ⁻⁴	1.8440 ⁻⁵	1.4122 ⁻⁸	9.3870 ⁻⁸	-1.9148 ⁻¹⁰	3.4478 ⁻⁸	2.6323 ⁻⁸	1.3434 ⁻⁶
$\mu_r^2 = 0.5 \mu_f^2$								
1.0 ⁻⁷	3.1361 ⁻⁵	-1.8232 ⁻⁵	6.8212 ⁻⁶	1.4192 ⁺²	-8.8075 ⁻⁵	6.9888 ⁺¹	6.9175 ⁺¹	1.0040 ⁺³
1.0 ⁻⁶	4.0428 ⁻⁴	1.5878 ⁻⁴	3.0618 ⁻⁵	6.8336 ⁺¹	-1.8570 ⁻⁴	3.3318 ⁺¹	3.2752 ⁺¹	4.6992 ⁺²
1.0 ⁻⁵	2.6243 ⁻³	1.4295 ⁻³	1.3000 ⁻⁴	3.2801 ⁺¹	-2.3602 ⁻⁴	1.5726 ⁺¹	1.5276 ⁺¹	2.1381 ⁺²
1.0 ⁻⁴	1.3458 ⁻²	7.8155 ⁻³	5.1314 ⁻⁴	1.5042 ⁺¹	3.9611 ⁻⁵	6.9878 ⁺⁰	6.6319 ⁺⁰	8.9170 ⁺¹
1.0 ⁻³	6.0011 ⁻²	3.4728 ⁻²	1.8548 ⁻³	6.3047 ⁺⁰	6.1053 ⁻⁴	2.7409 ⁺⁰	2.4648 ⁺⁰	3.1498 ⁺¹
1.0 ⁻²	2.3206 ⁻¹	1.3018 ⁻¹	5.9593 ⁻³	2.2634 ⁺⁰	1.9681 ⁻⁴	8.5182 ⁻¹	6.6355 ⁻¹	8.1950 ⁺⁰
1.0 ⁻¹	5.5087 ⁻¹	2.7116 ⁻¹	1.0130 ⁻²	3.8935 ⁻¹	-3.0333 ⁻⁴	1.1393 ⁻¹	5.9975 ⁻²	9.0489 ⁻¹
3.0 ⁻¹	3.4987 ⁻¹	1.2993 ⁻¹	3.0140 ⁻³	3.5489 ⁻²	-4.1682 ⁻⁵	9.1436 ⁻³	3.4154 ⁻³	8.4375 ⁻²
5.0 ⁻¹	1.2088 ⁻¹	3.1453 ⁻²	3.7731 ⁻⁴	2.4189 ⁻³	-3.6076 ⁻⁶	5.9738 ⁻⁴	1.9041 ⁻⁴	8.1628 ⁻³
7.0 ⁻¹	2.0030 ⁻²	3.0824 ⁻³	1.3409 ⁻⁵	5.8135 ⁻⁵	-1.2487 ⁻⁷	1.4967 ⁻⁵	5.6246 ⁻⁶	3.9290 ⁻⁴
9.0 ⁻¹	3.4739 ⁻⁴	1.8076 ⁻⁵	1.3844 ⁻⁸	1.3960 ⁻⁷	-2.2058 ⁻¹⁰	5.7593 ⁻⁸	4.9622 ⁻⁸	1.3364 ⁻⁶

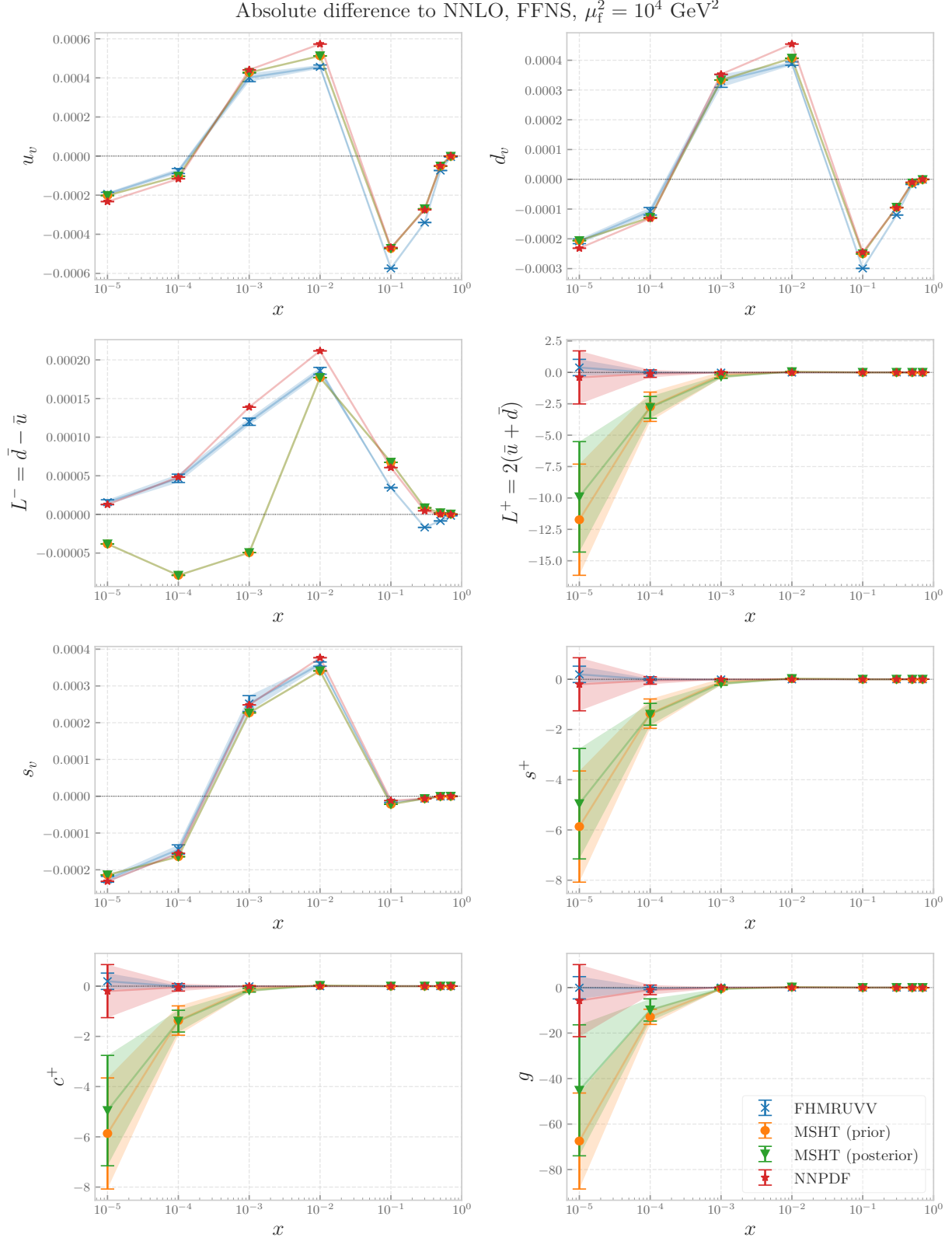


Figure 1: Absolute difference of the aN³LO evolution with respect to the NNLO, for the initial conditions and the input parton distributions given in Sec. 3.1 with the FFNS settings. We display results for FHMRUVV (blue), MSHT prior (orange), MSHT posterior (green) and NNPDF (red) approximations. The displayed FHMRUVV result is averaged between the values of the MSHT20 and NNPDF evolution code.

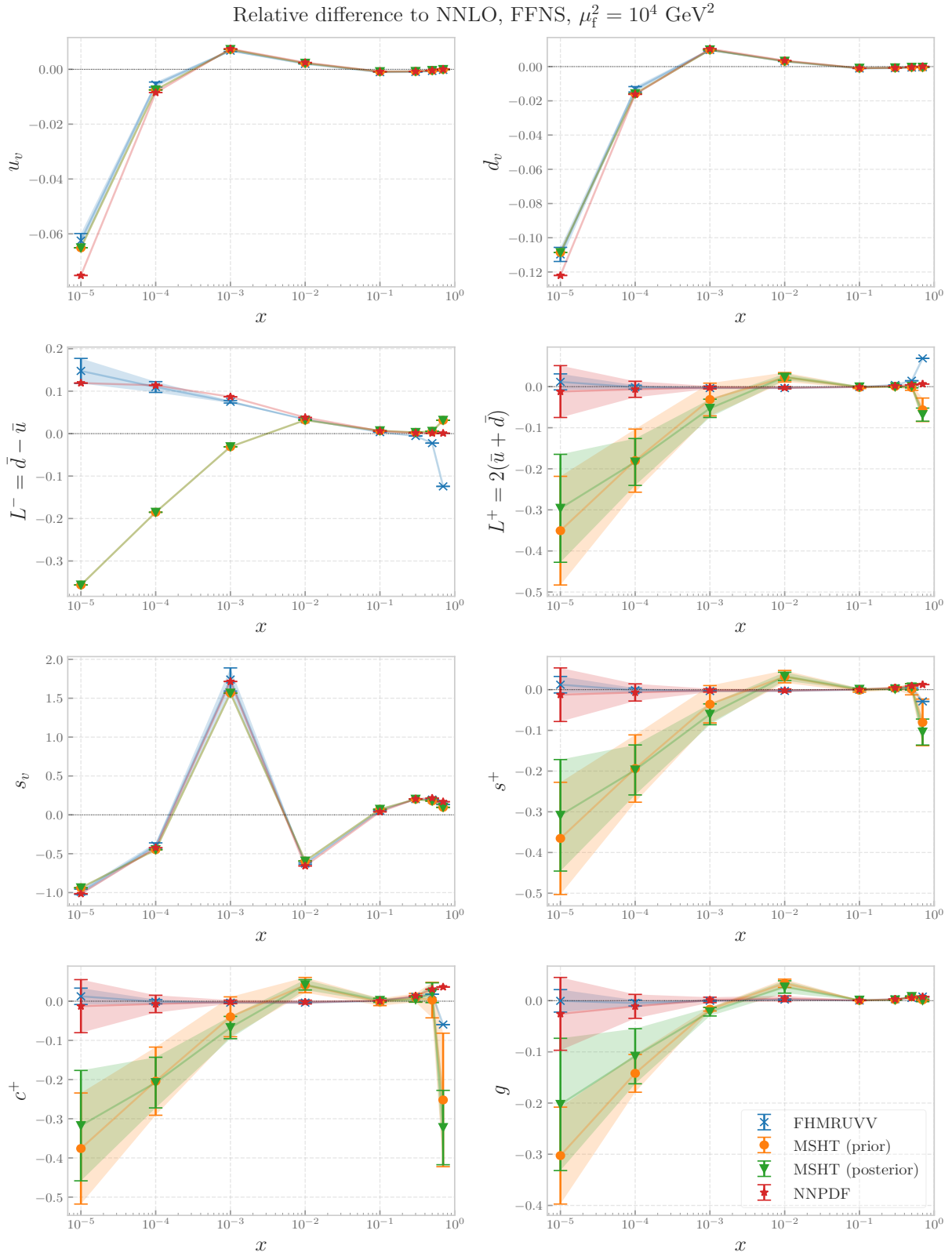


Figure 2: Same as Fig. 1, but now displaying the relative difference with respect to the NNLO evolution.

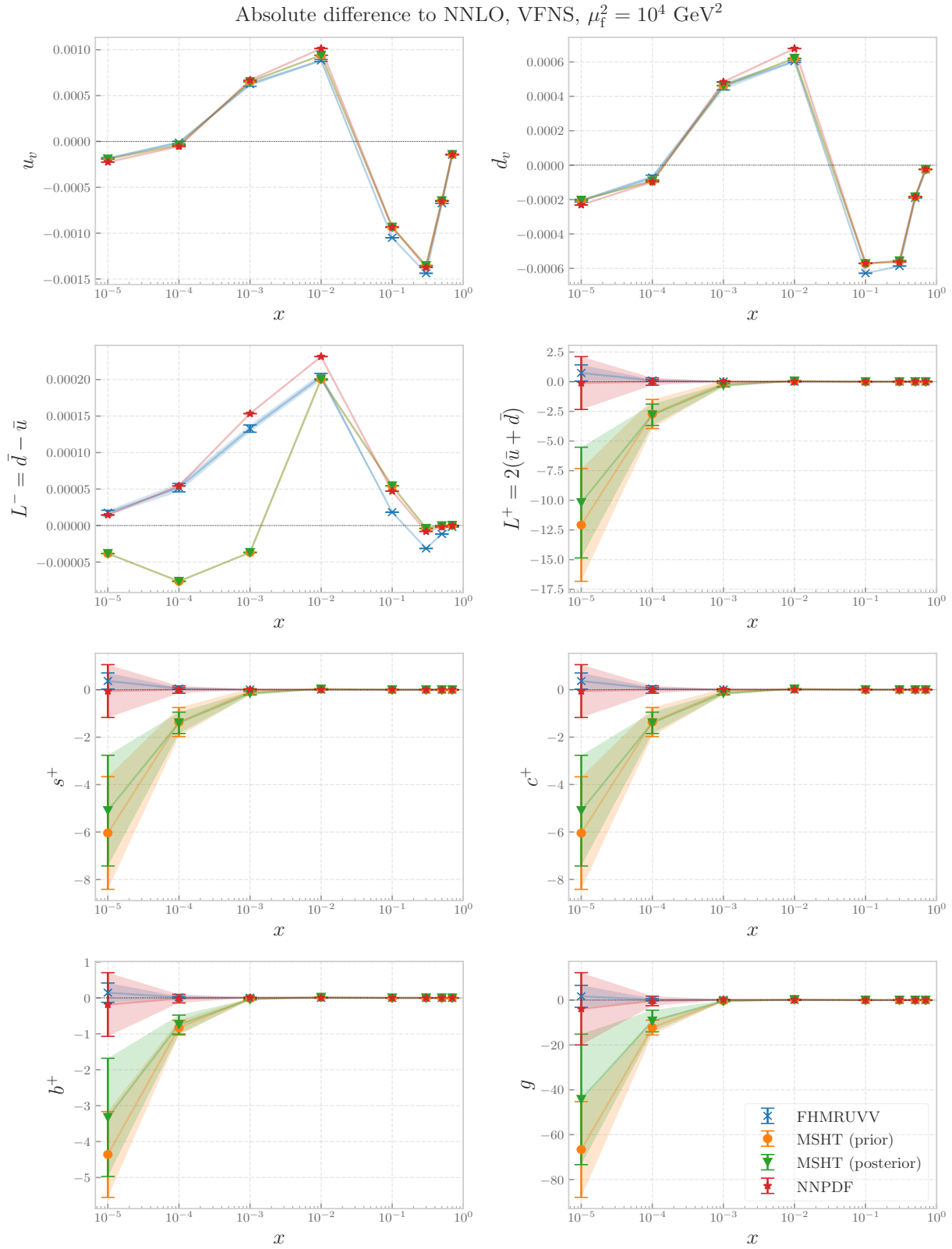


Figure 3: Same as Fig. 1, but now for VFNS evolution settings.

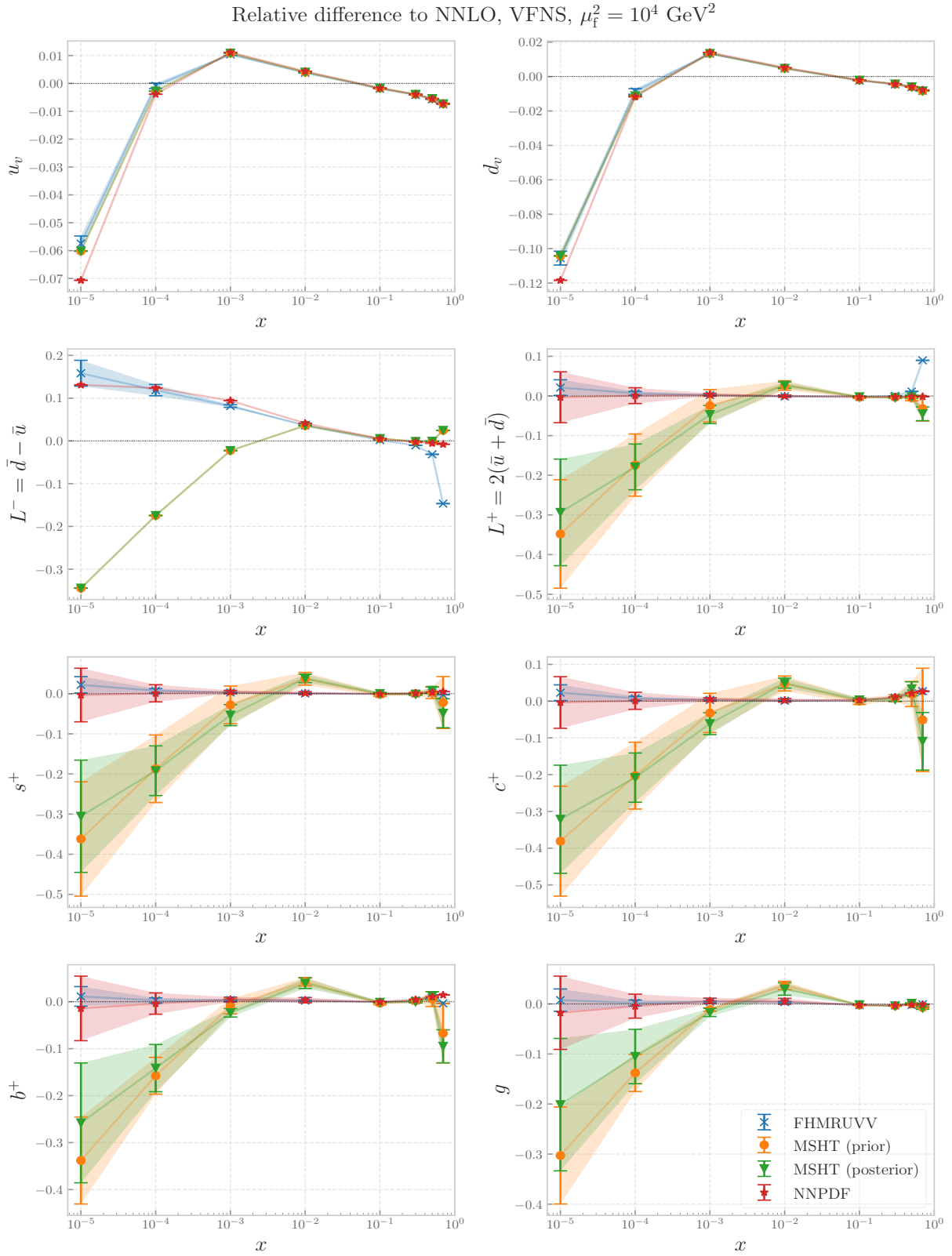


Figure 4: Same as Fig. 2, but now for VFNS evolution settings.

Table 6: Results for the VFNS aN³LO evolution for the initial conditions and the input parton distributions given in Sec. 3.1, with the FHMRUVV splitting functions approximation and the MSHT20aN3LO code.

FHMRUVV in MSHT20aN3LO, $n_f = 3 \dots 5$, $\mu_f^2 = 10^4 \text{ GeV}^2$								
x	xu_v	xd_v	xL_-	xL_+	xs_+	xc_+	xb_+	xg
$\mu_r^2 = \mu_f^2$								
1.0^{-7}	1.1639^{-4}	5.5630^{-5}	8.3396^{-6}	1.5915^{+2}	7.8505^{+1}	7.6906^{+1}	6.4245^{+1}	1.0973^{+3}
1.0^{-6}	6.0389^{-4}	3.3257^{-4}	3.2692^{-5}	7.6153^{+1}	3.7227^{+1}	3.6062^{+1}	2.9625^{+1}	5.0544^{+2}
1.0^{-5}	3.0183^{-3}	1.7563^{-3}	1.2872^{-4}	3.5490^{+1}	1.7071^{+1}	1.6248^{+1}	1.3056^{+1}	2.2175^{+2}
1.0^{-4}	1.4024^{-2}	8.2158^{-3}	4.8879^{-4}	1.5724^{+1}	7.3290^{+0}	6.7755^{+0}	5.2766^{+0}	8.8931^{+1}
1.0^{-3}	6.0636^{-2}	3.4976^{-2}	1.7596^{-3}	6.4308^{+0}	2.8038^{+0}	2.4567^{+0}	1.8204^{+0}	3.0517^{+1}
1.0^{-2}	2.3325^{-1}	1.3055^{-1}	5.8026^{-3}	2.2752^{+0}	8.5774^{-1}	6.6785^{-1}	4.5172^{-1}	7.8160^{+0}
1.0^{-1}	5.4876^{-1}	2.6967^{-1}	9.9483^{-3}	3.8453^{-1}	1.1219^{-1}	6.4546^{-2}	3.7236^{-2}	8.5051^{-1}
3.0^{-1}	3.4472^{-1}	1.2772^{-1}	2.9024^{-3}	3.4706^{-2}	8.8422^{-3}	4.0495^{-3}	2.1095^{-3}	7.8671^{-2}
5.0^{-1}	1.1798^{-1}	3.0615^{-2}	3.4653^{-4}	2.3789^{-3}	5.6438^{-4}	2.4370^{-4}	1.2144^{-4}	7.6252^{-3}
7.0^{-1}	1.9335^{-2}	2.9654^{-3}	9.2473^{-6}	6.2100^{-5}	1.2548^{-5}	5.9902^{-6}	2.9754^{-6}	3.7046^{-4}
9.0^{-1}	3.3148^{-4}	1.6782^{-5}	-6.3382^{-8}	1.8337^{-7}	6.2892^{-9}	8.4763^{-9}	3.5330^{-9}	1.1753^{-6}

(which is largely at small x) can be regarded as a measure of the uncertainty. This is generally very small on an absolute scale due to the smallness of the corresponding non-singlet flavor combinations. Figs. 1 and 2 for the evolution in the FFNS scheme show that all the N³LO approximations provide consistent results in the data region of $x \gtrsim 10^{-3}$, with at most few percent differences relative to NNLO and often less for most PDF flavor combinations, whilst absolute differences are smaller still. There are some remaining differences in the small- x region where the uncertainties of the individual approximations also grow due to unknown small- x logarithms and so the theoretical uncertainties are larger. Thus in the kinematic range of the LHC, the benchmark numbers for the aN³LO evolution demonstrate good perturbative convergence and a significant reduction of the residual theoretical uncertainty. Hence, they should be sufficient for most collider-physics applications. Similar findings are observed in Figs. 3 and 4 for the evolution in the VFNS scheme.

As a final study, in order to check the stability of the DGLAP kernels at different QCD orders, we investigate the effect of different DGLAP solution methods [41], called *exact* and *truncated*, which differ by the inclusion of higher order terms. The former is utilised by MSHT in their x -space implementation and the latter by NNPDF in their Mellin space implementation. In the NNPDF code either method of solution is implemented and we utilise this to compare the impact of this difference. From Fig. 5 we observe that, as higher orders in the splitting functions are included the difference between the different solution methods is smaller, indicating a good perturbative convergence. This is visible both for non-singlet like distributions (L^-) and singlet-like (L^+ and g).

4 Conclusions and Outlook

The study has shown excellent agreement between MSHT and NNPDF evolution when exactly the same versions of the N³LO splitting functions are used. In addition, it is observed that the differences for $x > 10^{-3}$ are very small when the distinct original estimates used in [43] and [46] are used. Moreover, the origin of the small differences in this region, and larger ones for smaller x is well understood in terms of differences in the approximate splitting functions. Hence, the study has been a success in this regard. Furthermore, we can see in Fig. 5 that there is also good convergence in the difference between the exact DGLAP evolution and the truncated solution method as the order of the equation used increases, and specifically that at N³LO this is also small fractions of a percent except at very small x or in very small non-singlet quark combinations. Thus, overall, we can have high confidence in our precision in PDF evolution at N³LO. However, there are

Table 7: Results for the VFNS aN³LO evolution for the initial conditions and the input parton distributions given in Sec. 3.1, with the FHMRUVV splitting functions approximation and the NNPDF code.

FHMRUVV in NNPDF, $n_f = 3 \dots 5$, $\mu_f^2 = 10^4 \text{ GeV}^2$								
x	xu_v	xd_v	xL_-	xL_+	xs_+	xc_+	xb_+	xg
$\mu_r^2 = \mu_f^2$								
1.0^{-7}	1.0347^{-4}	4.7296^{-5}	7.9869^{-6}	1.5846^{+2}	7.8162^{+1}	7.6575^{+1}	6.3898^{+1}	1.0941^{+3}
1.0^{-6}	5.8850^{-4}	3.2158^{-4}	3.2458^{-5}	7.5933^{+1}	3.7117^{+1}	3.5959^{+1}	2.9511^{+1}	5.0475^{+2}
1.0^{-5}	2.9963^{-3}	1.7380^{-3}	1.2878^{-4}	3.5427^{+1}	1.7039^{+1}	1.6221^{+1}	1.3021^{+1}	2.2169^{+2}
1.0^{-4}	1.3998^{-2}	8.1908^{-3}	4.8992^{-4}	1.5705^{+1}	7.3201^{+0}	6.7688^{+0}	5.2666^{+0}	8.8942^{+1}
1.0^{-3}	6.0651^{-2}	3.4981^{-2}	1.7651^{-3}	6.4269^{+0}	2.8020^{+0}	2.4559^{+0}	1.8183^{+0}	3.0527^{+1}
1.0^{-2}	2.3339^{-1}	1.3065^{-1}	5.8248^{-3}	2.2744^{+0}	8.5749^{-1}	6.6796^{-1}	4.5145^{-1}	7.8173^{+0}
1.0^{-1}	5.4900^{-1}	2.6978^{-1}	1.0007^{-2}	3.8425^{-1}	1.1225^{-1}	6.4658^{-2}	3.7274^{-2}	8.5068^{-1}
3.0^{-1}	3.4485^{-1}	1.2776^{-1}	2.9491^{-3}	3.4522^{-2}	8.8517^{-3}	4.0601^{-3}	2.1150^{-3}	7.8667^{-2}
5.0^{-1}	1.1803^{-1}	3.0629^{-2}	3.6563^{-4}	2.3176^{-3}	5.6611^{-4}	2.4371^{-4}	1.2203^{-4}	7.6246^{-3}
7.0^{-1}	1.9344^{-2}	2.9683^{-3}	1.2839^{-5}	5.2471^{-5}	1.2749^{-5}	5.9801^{-6}	3.0847^{-6}	3.7020^{-4}
9.0^{-1}	3.2955^{-4}	1.7232^{-5}	1.0350^{-8}	5.5700^{-8}	1.9893^{-8}	1.4418^{-8}	7.7074^{-9}	1.2669^{-6}
$\mu_r^2 = 2 \mu_f^2$								
1.0^{-7}	1.1909^{-4}	6.5970^{-5}	6.8741^{-6}	1.4822^{+2}	7.3036^{+1}	7.1713^{+1}	6.0917^{+1}	1.0484^{+3}
1.0^{-6}	6.1538^{-4}	3.5855^{-4}	2.8837^{-5}	7.2880^{+1}	3.5589^{+1}	3.4609^{+1}	2.8797^{+1}	4.9380^{+2}
1.0^{-5}	2.9935^{-3}	1.7685^{-3}	1.1716^{-4}	3.4488^{+1}	1.6568^{+1}	1.5861^{+1}	1.2847^{+1}	2.1891^{+2}
1.0^{-4}	1.3780^{-2}	8.0806^{-3}	4.5472^{-4}	1.5398^{+1}	7.1650^{+0}	6.6722^{+0}	5.2108^{+0}	8.8043^{+1}
1.0^{-3}	5.9855^{-2}	3.4495^{-2}	1.6768^{-3}	6.3396^{+0}	2.7570^{+0}	2.4315^{+0}	1.7991^{+0}	3.0254^{+1}
1.0^{-2}	2.3216^{-1}	1.3001^{-1}	5.6938^{-3}	2.2639^{+0}	8.5089^{-1}	6.6127^{-1}	4.4740^{-1}	7.7845^{+0}
1.0^{-1}	5.5058^{-1}	2.7082^{-1}	1.0018^{-2}	3.8658^{-1}	1.1275^{-1}	6.3045^{-2}	3.7010^{-2}	8.5589^{-1}
3.0^{-1}	3.4779^{-1}	1.2900^{-1}	2.9789^{-3}	3.4935^{-2}	8.9514^{-3}	3.8484^{-3}	2.0908^{-3}	7.9589^{-2}
5.0^{-1}	1.1956^{-1}	3.1068^{-2}	3.7136^{-4}	2.3531^{-3}	5.7380^{-4}	2.2346^{-4}	1.1959^{-4}	7.7331^{-3}
7.0^{-1}	1.9700^{-2}	3.0274^{-3}	1.3120^{-5}	5.3288^{-5}	1.2861^{-5}	5.2550^{-6}	2.9616^{-6}	3.7634^{-4}
9.0^{-1}	3.3899^{-4}	1.7735^{-5}	1.0779^{-8}	5.3917^{-8}	1.8648^{-8}	1.2598^{-8}	6.8401^{-9}	1.2945^{-6}
$\mu_r^2 = 0.5 \mu_f^2$								
1.0^{-7}	4.5549^{-5}	-1.3718^{-5}	9.7980^{-6}	1.8191^{+2}	8.9889^{+1}	8.7771^{+1}	7.1481^{+1}	1.2220^{+3}
1.0^{-6}	4.5429^{-4}	1.7961^{-4}	3.7731^{-5}	8.1754^{+1}	4.0029^{+1}	3.8512^{+1}	3.1146^{+1}	5.3370^{+2}
1.0^{-5}	2.7921^{-3}	1.5132^{-3}	1.4423^{-4}	3.6683^{+1}	1.7669^{+1}	1.6627^{+1}	1.3311^{+1}	2.2754^{+2}
1.0^{-4}	1.3969^{-2}	8.0954^{-3}	5.3559^{-4}	1.5967^{+1}	7.4522^{+0}	6.7828^{+0}	5.3273^{+0}	9.0292^{+1}
1.0^{-3}	6.1375^{-2}	3.5488^{-2}	1.8845^{-3}	6.4753^{+0}	2.8278^{+0}	2.4397^{+0}	1.8381^{+0}	3.0881^{+1}
1.0^{-2}	2.3477^{-1}	1.3154^{-1}	6.0188^{-3}	2.2728^{+0}	8.5849^{-1}	6.6835^{-1}	4.5573^{-1}	7.8549^{+0}
1.0^{-1}	5.4786^{-1}	2.6903^{-1}	1.0032^{-2}	3.8184^{-1}	1.1169^{-1}	6.7883^{-2}	3.7592^{-2}	8.4316^{-1}
3.0^{-1}	3.4245^{-1}	1.2676^{-1}	2.9274^{-3}	3.4233^{-2}	8.8003^{-3}	4.5516^{-3}	2.1528^{-3}	7.7581^{-2}
5.0^{-1}	1.1677^{-1}	3.0270^{-2}	3.6111^{-4}	2.2949^{-3}	5.6319^{-4}	2.8913^{-4}	1.2584^{-4}	7.5139^{-3}
7.0^{-1}	1.9055^{-2}	2.9204^{-3}	1.2615^{-5}	5.1944^{-5}	1.2734^{-5}	7.4168^{-6}	3.2604^{-6}	3.6473^{-4}
9.0^{-1}	3.2199^{-4}	1.6832^{-5}	9.9709^{-9}	5.9105^{-8}	2.1920^{-8}	1.7299^{-8}	8.9014^{-9}	1.2443^{-6}

Table 8: Results for the VFNS aN³LO evolution for the initial conditions and the input parton distributions given in Sec. 3.1, with the MSHT20aN3LO prior splitting functions approximation.

MSHT20aN3LO prior, $n_f = 3 \dots 5$, $\mu_f^2 = 10^4 \text{ GeV}^2$								
x	xu_v	xd_v	xL_-	xL_+	xs_+	xc_+	xb_+	xg
$\mu_r^2 = \mu_f^2$								
1.0 ⁻⁷	1.2800 ⁻⁴	7.0312 ⁻⁵	2.6923 ⁻⁶	5.4816 ⁺¹	2.6337 ⁺¹	2.4743 ⁺¹	2.1448 ⁺¹	3.9567 ⁺²
1.0 ⁻⁶	6.1135 ⁻⁴	3.4762 ⁻⁴	1.3705 ⁻⁵	3.5854 ⁺¹	1.7076 ⁺¹	1.5914 ⁺¹	1.4042 ⁺¹	2.5956 ⁺²
1.0 ⁻⁵	2.9987 ⁻³	1.7496 ⁻³	7.2860 ⁻⁵	2.2642 ⁺¹	1.0646 ⁺¹	9.8250 ⁺⁰	8.5356 ⁺⁰	1.5346 ⁺²
1.0 ⁻⁴	1.3984 ⁻²	8.1825 ⁻³	3.6107 ⁻⁴	1.2894 ⁺¹	5.9135 ⁺⁰	5.3608 ⁺⁰	4.4296 ⁺⁰	7.6535 ⁺¹
1.0 ⁻³	6.0671 ⁻²	3.4982 ⁻²	1.5927 ⁻³	6.2577 ⁺⁰	2.7167 ⁺⁰	2.3699 ⁺⁰	1.7961 ⁺⁰	3.0052 ⁺¹
1.0 ⁻²	2.3338 ⁻¹	1.3062 ⁻¹	5.8105 ⁻³	2.3375 ⁺⁰	8.8903 ⁻¹	6.9912 ⁻¹	4.6967 ⁻¹	8.0754 ⁺⁰
1.0 ⁻¹	5.4900 ⁻¹	2.6978 ⁻¹	1.0014 ⁻²	3.8396 ⁻¹	1.1210 ⁻¹	6.4442 ⁻²	3.7165 ⁻²	8.5071 ⁻¹
3.0 ⁻¹	3.4487 ⁻¹	1.2777 ⁻¹	2.9532 ⁻³	3.4489 ⁻²	8.8453 ⁻³	4.0478 ⁻³	2.1095 ⁻³	7.8598 ⁻²
5.0 ⁻¹	1.1803 ⁻¹	3.0628 ⁻²	3.6736 ⁻⁴	2.3104 ⁻³	5.6565 ⁻⁴	2.4326 ⁻⁴	1.2147 ⁻⁴	7.6445 ⁻³
7.0 ⁻¹	1.9343 ⁻²	2.9667 ⁻³	1.3259 ⁻⁵	5.0879 ⁻⁵	1.2404 ⁻⁵	5.5290 ⁻⁶	2.8363 ⁻⁶	3.6793 ⁻⁴
9.0 ⁻¹	3.3162 ⁻⁴	1.6789 ⁻⁵	1.5757 ⁻⁸	6.7806 ⁻⁹	5.6859 ⁻⁹	1.8831 ⁻⁹	1.7371 ⁻⁹	1.1316 ⁻⁶

Table 9: Results for the VFNS aN³LO evolution for the initial conditions and the input parton distributions given in Sec. 3.1, with the MSHT20aN3LO posterior splitting functions approximation.

MSHT20aN3LO posterior, $n_f = 3 \dots 5$, $\mu_f^2 = 10^4 \text{ GeV}^2$								
x	xu_v	xd_v	xL_-	xL_+	xs_+	xc_+	xb_+	xg
$\mu_r^2 = \mu_f^2$								
1.0 ⁻⁷	1.2800 ⁻⁴	7.0312 ⁻⁵	2.6923 ⁻⁶	8.9533 ⁺¹	4.3695 ⁺¹	4.2104 ⁺¹	3.7572 ⁺¹	7.1965 ⁺²
1.0 ⁻⁶	6.1135 ⁻⁴	3.4762 ⁻⁴	1.3705 ⁻⁵	4.6946 ⁺¹	2.2622 ⁺¹	2.1462 ⁺¹	1.9346 ⁺¹	3.6755 ⁺²
1.0 ⁻⁵	2.9987 ⁻³	1.7496 ⁻³	7.2860 ⁻⁵	2.4866 ⁺¹	1.1758 ⁺¹	1.0938 ⁺¹	9.7679 ⁺⁰	1.8033 ⁺²
1.0 ⁻⁴	1.3984 ⁻²	8.1825 ⁻³	3.6107 ⁻⁴	1.2832 ⁺¹	5.8825 ⁺⁰	5.3303 ⁺⁰	4.5420 ⁺⁰	8.0208 ⁺¹
1.0 ⁻³	6.0671 ⁻²	3.4982 ⁻²	1.5927 ⁻³	6.0992 ⁺⁰	2.6374 ⁺⁰	2.2908 ⁺⁰	1.7687 ⁺⁰	2.9886 ⁺¹
1.0 ⁻²	2.3338 ⁻¹	1.3062 ⁻¹	5.8105 ⁻³	2.3390 ⁺⁰	8.8977 ⁻¹	6.9985 ⁻¹	4.6773 ⁻¹	8.0041 ⁺⁰
1.0 ⁻¹	5.4900 ⁻¹	2.6978 ⁻¹	1.0014 ⁻²	3.8449 ⁻¹	1.1236 ⁻¹	6.4711 ⁻²	3.7240 ⁻²	8.5137 ⁻¹
3.0 ⁻¹	3.4487 ⁻¹	1.2777 ⁻¹	2.9532 ⁻³	3.4457 ⁻²	8.8291 ⁻³	4.0316 ⁻³	2.1054 ⁻³	7.8573 ⁻²
5.0 ⁻¹	1.1803 ⁻¹	3.0628 ⁻²	3.6736 ⁻⁴	2.3177 ⁻³	5.6933 ⁻⁴	2.4693 ⁻⁴	1.2236 ⁻⁴	7.6478 ⁻³
7.0 ⁻¹	1.9343 ⁻²	2.9667 ⁻³	1.3259 ⁻⁵	5.0141 ⁻⁵	1.2035 ⁻⁵	5.1605 ⁻⁶	2.7464 ⁻⁶	3.6765 ⁻⁴
9.0 ⁻¹	3.3162 ⁻⁴	1.6789 ⁻⁵	1.5757 ⁻⁸	-3.6339 ⁻⁹	4.7866 ⁻¹⁰	-3.3152 ⁻⁹	4.9166 ⁻¹⁰	1.1249 ⁻⁶

Table 10: Results for the VFNS aN³LO evolution for the initial conditions and the input parton distributions given in Sec. 3.1, with the NNPDF splitting functions approximation.

NNPDF, $n_f = 3 \dots 5$, $\mu_f^2 = 10^4 \text{ GeV}^2$								
x	xu_v	xd_v	xL_-	xL_+	xs_+	xc_+	xb_+	xg
$\mu_r^2 = \mu_f^2$								
1.0^{-7}	9.6344^{-5}	4.3393^{-5}	6.7727^{-6}	1.4525^{+2}	7.1554^{+1}	6.9967^{+1}	5.8515^{+1}	1.0001^{+3}
1.0^{-6}	5.7167^{-4}	3.1255^{-4}	3.0007^{-5}	7.2074^{+1}	3.5187^{+1}	3.4029^{+1}	2.7983^{+1}	4.7809^{+2}
1.0^{-5}	2.9653^{-3}	1.7220^{-3}	1.2572^{-4}	3.4609^{+1}	1.6630^{+1}	1.5812^{+1}	1.2709^{+1}	2.1616^{+2}
1.0^{-4}	1.3969^{-2}	8.1776^{-3}	4.9163^{-4}	1.5624^{+1}	7.2793^{+0}	6.7280^{+0}	5.2371^{+0}	8.8369^{+1}
1.0^{-3}	6.0687^{-2}	3.5003^{-2}	1.7829^{-3}	6.4348^{+0}	2.8060^{+0}	2.4600^{+0}	1.8214^{+0}	3.0571^{+1}
1.0^{-2}	2.3345^{-1}	1.3068^{-1}	5.8414^{-3}	2.2757^{+0}	8.5822^{-1}	6.6869^{-1}	4.5199^{-1}	7.8282^{+0}
1.0^{-1}	5.4900^{-1}	2.6978^{-1}	1.0007^{-2}	3.8424^{-1}	1.1224^{-1}	6.4654^{-2}	3.7272^{-2}	8.5064^{-1}
3.0^{-1}	3.4485^{-1}	1.2776^{-1}	2.9491^{-3}	3.4522^{-2}	8.8518^{-3}	4.0602^{-3}	2.1151^{-3}	7.8668^{-2}
5.0^{-1}	1.1803^{-1}	3.0629^{-2}	3.6564^{-4}	2.3176^{-3}	5.6610^{-4}	2.4370^{-4}	1.2202^{-4}	7.6247^{-3}
7.0^{-1}	1.9344^{-2}	2.9683^{-3}	1.2840^{-5}	5.2470^{-5}	1.2749^{-5}	5.9804^{-6}	3.0846^{-6}	3.7016^{-4}
9.0^{-1}	3.2955^{-4}	1.7232^{-5}	1.0383^{-8}	5.5649^{-8}	1.9895^{-8}	1.4420^{-8}	7.7216^{-9}	1.2702^{-6}
$\mu_r^2 = 2 \mu_f^2$								
1.0^{-7}	1.1488^{-4}	6.3669^{-5}	6.1597^{-6}	1.4072^{+2}	6.9288^{+1}	6.7964^{+1}	5.7807^{+1}	9.9296^{+2}
1.0^{-6}	6.0542^{-4}	3.5321^{-4}	2.7394^{-5}	7.0695^{+1}	3.4496^{+1}	3.3517^{+1}	2.7917^{+1}	4.7808^{+2}
1.0^{-5}	2.9750^{-3}	1.7590^{-3}	1.1536^{-4}	3.4025^{+1}	1.6337^{+1}	1.5629^{+1}	1.2667^{+1}	2.1563^{+2}
1.0^{-4}	1.3763^{-2}	8.0727^{-3}	4.5575^{-4}	1.5351^{+1}	7.1417^{+0}	6.6490^{+0}	5.1938^{+0}	8.7698^{+1}
1.0^{-3}	5.9877^{-2}	3.4508^{-2}	1.6874^{-3}	6.3441^{+0}	2.7592^{+0}	2.4338^{+0}	1.8009^{+0}	3.0279^{+1}
1.0^{-2}	2.3219^{-1}	1.3002^{-1}	5.7037^{-3}	2.2647^{+0}	8.5130^{-1}	6.6169^{-1}	4.4771^{-1}	7.7911^{+0}
1.0^{-1}	5.5058^{-1}	2.7082^{-1}	1.0017^{-2}	3.8658^{-1}	1.1275^{-1}	6.3043^{-2}	3.7008^{-2}	8.5586^{-1}
3.0^{-1}	3.4779^{-1}	1.2900^{-1}	2.9789^{-3}	3.4936^{-2}	8.9514^{-3}	3.8485^{-3}	2.0909^{-3}	7.9590^{-2}
5.0^{-1}	1.1956^{-1}	3.1068^{-2}	3.7137^{-4}	2.3530^{-3}	5.7380^{-4}	2.2346^{-4}	1.1958^{-4}	7.7332^{-3}
7.0^{-1}	1.9700^{-2}	3.0274^{-3}	1.3120^{-5}	5.3287^{-5}	1.2861^{-5}	5.2552^{-6}	2.9616^{-6}	3.7631^{-4}
9.0^{-1}	3.3899^{-4}	1.7735^{-5}	1.0800^{-8}	5.3886^{-8}	1.8649^{-8}	1.2599^{-8}	6.8475^{-9}	1.2968^{-6}
$\mu_r^2 = 0.5 \mu_f^2$								
1.0^{-7}	3.1561^{-5}	-2.1401^{-5}	7.4030^{-6}	1.5487^{+2}	7.6366^{+1}	7.4248^{+1}	6.0692^{+1}	1.0369^{+3}
1.0^{-6}	4.2125^{-4}	1.6183^{-4}	3.2892^{-5}	7.3820^{+1}	3.6062^{+1}	3.4545^{+1}	2.8065^{+1}	4.8122^{+2}
1.0^{-5}	2.7315^{-3}	1.4819^{-3}	1.3816^{-4}	3.4999^{+1}	1.6827^{+1}	1.5785^{+1}	1.2679^{+1}	2.1672^{+2}
1.0^{-4}	1.3911^{-2}	8.0700^{-3}	5.3883^{-4}	1.5800^{+1}	7.3686^{+0}	6.6992^{+0}	5.2677^{+0}	8.9197^{+1}
1.0^{-3}	6.1446^{-2}	3.5531^{-2}	1.9191^{-3}	6.4917^{+0}	2.8361^{+0}	2.4480^{+0}	1.8444^{+0}	3.0971^{+1}
1.0^{-2}	2.3489^{-1}	1.3159^{-1}	6.0512^{-3}	2.2756^{+0}	8.5998^{-1}	6.6984^{-1}	4.5683^{-1}	7.8758^{+0}
1.0^{-1}	5.4786^{-1}	2.6903^{-1}	1.0031^{-2}	3.8183^{-1}	1.1168^{-1}	6.7876^{-2}	3.7587^{-2}	8.4307^{-1}
3.0^{-1}	3.4245^{-1}	1.2676^{-1}	2.9275^{-3}	3.4234^{-2}	8.8006^{-3}	4.5518^{-3}	2.1530^{-3}	7.7584^{-2}
5.0^{-1}	1.1677^{-1}	3.0270^{-2}	3.6112^{-4}	2.2948^{-3}	5.6318^{-4}	2.8912^{-4}	1.2583^{-4}	7.5141^{-3}
7.0^{-1}	1.9055^{-2}	2.9204^{-3}	1.2616^{-5}	5.1942^{-5}	1.2735^{-5}	7.4174^{-6}	3.2603^{-6}	3.6466^{-4}
9.0^{-1}	3.2199^{-4}	1.6832^{-5}	1.0033^{-8}	5.9017^{-8}	2.1925^{-8}	1.7304^{-8}	8.9339^{-9}	1.2496^{-6}

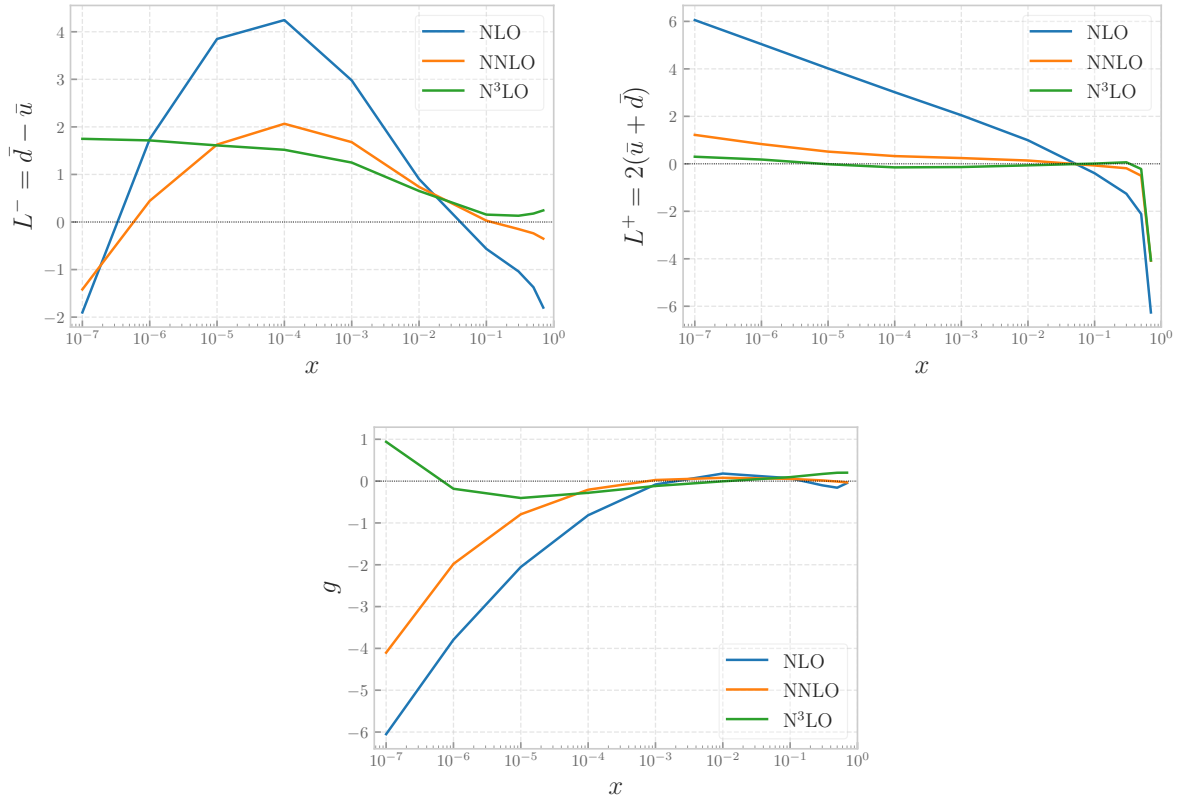


Figure 5: Relative difference in percent between the exact and truncated solution of the DGLAP evolution at different perturbative orders. We adopt the same evolution and boundary condition as in the benchmark exercise and display the result for the non-singlet quark combinations L^- , L^+ and the gluon g .

obvious further avenues for exploration.

As mentioned in Section 2.2, the $\mathcal{O}(\alpha_S^3)$ versions of the OMEs for transition across heavy flavour transition points are now complete [27, 29, 30, 35, 75, 76, 77, 78, 79, 80], though the final parts only became available while our study was already well underway. Also, not all parts are currently in an easily usable form. Hence we only included the transition matrix elements up to $\mathcal{O}(\alpha_S^2)$, i.e. NNLO in this study. In the future we can consider the effects of improving upon this.

There are also effects of additional information [14, 17, 18, 19], such as moments, computed since the original MSHT estimates of the splitting functions. We have studied the effect of the benchmark evolution of MSHT including instead the FHMURVV determination of the splitting functions, but it would be of at least as much interest to examine the effect of this update in a full PDF fit. Indeed, MSHT have preliminary results [81] which show changes mainly in the gluon distribution, but remaining within the uncertainty band of the original MSHT determination. These bring the change in the MSHT aN³LO gluon compared to that at NNLO somewhat closer to that observed by NNPDF, which also observes a dip in the gluon around $x \sim 0.01$ but of reduced magnitude. To be explicit the change in the dip at $x \sim 0.01$ is reduced by about 1.5%. Finally very recently additional moments for P_{gq} were determined in [20], these are therefore included in neither of the PDF groups approximations and so it would be interesting to see the effect on the PDFs, and corresponding improvements in agreement. As such, the level of variation in N³LO evolution illustrated in Figs. 1 to 4 is very much an upper estimate, which will be reduced when all up to date information which can be used to estimate N³LO splitting functions now available is used by all groups. Uncertainties from other sources, e.g. limitations in the precision of cross sections to use together with N³LO evolution in PDF extractions, is a possible study for the future. In addition, there are also methodological differences in the implementation of the associated theoretical uncertainties.

However, given that the results in this report already show a good level of convergence in the most important regions for N³LO PDF evolution phenomenological studies, we can conclude that at least as far as an understanding of this evolution is concerned, we are reaching a point where relevant uncertainties are very small and are estimated reliably.

Acknowledgements

T. C. acknowledges that this project has received funding from the European Research Council (ERC) under the European Union’s Horizon 2020 research and innovation programme (Grant agreement No. 101002090 COLORFREE). L. H.-L. and R.S. T. thank STFC for support via grant awards ST/T000856/1 and ST/X000516/1. F. H. is supported by the Academy of Finland project 358090 and is funded as a part of the Center of Excellence in Quark Matter of the Academy of Finland, project 346326. S. M. acknowledges the ERC Advanced Grant 101095857 Conformal-EIC.

References

- [1] W. Giele et al., *The QCD / SM working group: Summary report*, [hep-ph/0204316](#).
- [2] M. Dittmar et al., *Working Group I: Parton distributions: Summary report for the HERA LHC Workshop Proceedings*, [hep-ph/0511119](#).
- [3] J. Andersen et al., *Les Houches 2023: Physics at TeV Colliders: Standard Model Working Group Report*, in *Physics of the TeV Scale and Beyond the Standard Model: Intensifying the Quest for New Physics*, 6, 2024, [2406.00708](#).
- [4] P. A. Baikov, K. G. Chetyrkin and J. H. Kühn, *Five-Loop Running of the QCD coupling constant*, *Phys. Rev. Lett.* **118** (2017) 082002 [[1606.08659](#)].
- [5] F. Herzog, B. Ruijl, T. Ueda, J. A. M. Vermaseren and A. Vogt, *The five-loop beta function of Yang-Mills theory with fermions*, *JHEP* **02** (2017) 090 [[1701.01404](#)].
- [6] K. G. Chetyrkin, G. Falcioni, F. Herzog and J. A. M. Vermaseren, *Five-loop renormalisation of QCD in covariant gauges*, *JHEP* **10** (2017) 179 [[1709.08541](#)].

- [7] T. Luthe, A. Maier, P. Marquard and Y. Schroder, *The five-loop Beta function for a general gauge group and anomalous dimensions beyond Feynman gauge*, *JHEP* **10** (2017) 166 [[1709.07718](#)].
- [8] S. Moch, J. A. M. Vermaseren and A. Vogt, *The Three loop splitting functions in QCD: The Nonsinglet case*, *Nucl. Phys. B* **688** (2004) 101 [[hep-ph/0403192](#)].
- [9] A. Vogt, S. Moch and J. A. M. Vermaseren, *The Three-loop splitting functions in QCD: The Singlet case*, *Nucl. Phys. B* **691** (2004) 129 [[hep-ph/0404111](#)].
- [10] S. Moch, B. Ruijl, T. Ueda, J. A. M. Vermaseren and A. Vogt, *Four-Loop Non-Singlet Splitting Functions in the Planar Limit and Beyond*, *JHEP* **10** (2017) 041 [[1707.08315](#)].
- [11] J. Davies, A. Vogt, B. Ruijl, T. Ueda and J. A. M. Vermaseren, *Large- n_f contributions to the four-loop splitting functions in QCD*, *Nucl. Phys. B* **915** (2017) 335 [[1610.07477](#)].
- [12] T. Gehrmann, A. von Manteuffel, V. Sotnikov and T.-Z. Yang, *Complete N_f^2 contributions to four-loop pure-singlet splitting functions*, *JHEP* **01** (2024) 029 [[2308.07958](#)].
- [13] T. Gehrmann, A. von Manteuffel, V. Sotnikov and T.-Z. Yang, *The $N_f C_F^3$ contribution to the non-singlet splitting function at four-loop order*, *Phys. Lett. B* **849** (2024) 138427 [[2310.12240](#)].
- [14] G. Falcioni, F. Herzog, S. Moch, J. Vermaseren and A. Vogt, *The double fermionic contribution to the four-loop quark-to-gluon splitting function*, *Phys. Lett. B* **848** (2024) 138351 [[2310.01245](#)].
- [15] S. Moch, B. Ruijl, T. Ueda, J. A. M. Vermaseren and A. Vogt, *On quartic colour factors in splitting functions and the gluon cusp anomalous dimension*, *Phys. Lett. B* **782** (2018) 627 [[1805.09638](#)].
- [16] S. Moch, B. Ruijl, T. Ueda, J. A. M. Vermaseren and A. Vogt, *Low moments of the four-loop splitting functions in QCD*, *Phys. Lett. B* **825** (2022) 136853 [[2111.15561](#)].
- [17] G. Falcioni, F. Herzog, S. Moch and A. Vogt, *Four-loop splitting functions in QCD – The quark-quark case*, *Phys. Lett. B* **842** (2023) 137944 [[2302.07593](#)].
- [18] G. Falcioni, F. Herzog, S. Moch and A. Vogt, *Four-loop splitting functions in QCD – The gluon-to-quark case*, *Phys. Lett. B* **846** (2023) 138215 [[2307.04158](#)].
- [19] S. Moch, B. Ruijl, T. Ueda, J. Vermaseren and A. Vogt, *Additional moments and x -space approximations of four-loop splitting functions in QCD*, [2310.05744](#).
- [20] G. Falcioni, F. Herzog, S. Moch, A. Pelloni and A. Vogt, *Four-loop splitting functions in QCD – The quark-to-gluon case*, [2404.09701](#).
- [21] Y. Schröder and M. Steinhauser, *Four-loop decoupling relations for the strong coupling*, *JHEP* **01** (2006) 051 [[hep-ph/0512058](#)].
- [22] K. G. Chetyrkin, J. H. Kühn and C. Sturm, *QCD decoupling at four loops*, *Nucl. Phys. B* **744** (2006) 121 [[hep-ph/0512060](#)].
- [23] M. Buza, Y. Matiounine, J. Smith, R. Migneron and W. L. van Neerven, *Heavy quark coefficient functions at asymptotic values $Q^2 \gg m^2$* , *Nucl. Phys. B* **472** (1996) 611 [[hep-ph/9601302](#)].
- [24] M. Buza, Y. Matiounine, J. Smith and W. L. van Neerven, *Charm electroproduction viewed in the variable flavor number scheme versus fixed order perturbation theory*, *Eur. Phys. J. C* **1** (1998) 301 [[hep-ph/9612398](#)].
- [25] J. Ablinger, J. Blumlein, S. Klein, C. Schneider and F. Wissbrock, *The $O(\alpha_s^3)$ Massive Operator Matrix Elements of $O(n_f)$ for the Structure Function $F_2(x, Q^2)$ and Transversity*, *Nucl. Phys. B* **844** (2011) 26 [[1008.3347](#)].
- [26] J. Ablinger, J. Blümlein, A. De Freitas, A. Hasselhuhn, A. von Manteuffel, M. Round et al., *The transition matrix element $a_{gq}(n)$ of the variable flavor number scheme at $O(\alpha_f^3)$* , *Nuclear Physics B* **882** (2014) 263–288.

- [27] J. Ablinger, A. Behring, J. Blümlein, A. De Freitas, A. von Manteuffel and C. Schneider, *The 3-loop pure singlet heavy flavor contributions to the structure function $F_2(x, Q^2)$ and the anomalous dimension*, *Nucl. Phys. B* **890** (2014) 48 [[1409.1135](#)].
- [28] J. Ablinger, A. Behring, J. Blümlein, A. De Freitas, A. von Manteuffel, C. Schneider et al., *The first-order factorizable contributions to the three-loop massive operator matrix elements $A_{Qg}^{(3)}$ and $\Delta A_{Qg}^{(3)}$* , *Nucl. Phys. B* **999** (2024) 116427 [[2311.00644](#)].
- [29] J. Ablinger, A. Behring, J. Blümlein, A. De Freitas, A. von Manteuffel, C. Schneider et al., *The non-first-order-factorizable contributions to the three-loop single-mass operator matrix elements $A_{Qg}^{(3)}$ and $\Delta A_{Qg}^{(3)}$* , [2403.00513](#).
- [30] H. Kawamura, N. A. Lo Presti, S. Moch and A. Vogt, *On the next-to-next-to-leading order QCD corrections to heavy-quark production in deep-inelastic scattering*, *Nucl. Phys. B* **864** (2012) 399 [[1205.5727](#)].
- [31] S. Alekhin, J. Blümlein, S. Moch and R. Placakyte, *Parton distribution functions, α_s , and heavy-quark masses for LHC Run II*, *Phys. Rev. D* **96** (2017) 014011 [[1701.05838](#)].
- [32] M. Buza, Y. Matiounine, J. Smith and W. L. van Neerven, *Charm electroproduction viewed in the variable flavor number scheme versus fixed order perturbation theory*, *Eur. Phys. J. C* **1** (1998) 301 [[hep-ph/9612398](#)].
- [33] J. Ablinger, J. Blümlein, A. De Freitas, C. Schneider and K. Schönwald, *The two-mass contribution to the three-loop pure singlet operator matrix element*, *Nucl. Phys. B* **927** (2018) 339 [[1711.06717](#)].
- [34] J. Ablinger, J. Blümlein, A. De Freitas, A. Goedicke, C. Schneider and K. Schönwald, *The Two-mass Contribution to the Three-Loop Gluonic Operator Matrix Element $A_{gg,Q}^{(3)}$* , *Nucl. Phys. B* **932** (2018) 129 [[1804.02226](#)].
- [35] J. Ablinger, A. Behring, J. Blümlein, A. De Freitas, A. Goedicke, A. von Manteuffel et al., *The unpolarized and polarized single-mass three-loop heavy flavor operator matrix elements $A_{gg,Q}$ and $\Delta A_{gg,Q}$* , *JHEP* **12** (2022) 134 [[2211.05462](#)].
- [36] J. Ablinger, J. Blümlein, A. De Freitas, A. Hasselhuhn, C. Schneider and F. Wißbrock, *Three Loop Massive Operator Matrix Elements and Asymptotic Wilson Coefficients with Two Different Masses*, *Nucl. Phys. B* **921** (2017) 585 [[1705.07030](#)].
- [37] APFEL collaboration, *APFEL: A PDF Evolution Library with QED corrections*, *Comput. Phys. Commun.* **185** (2014) 1647 [[1310.1394](#)].
- [38] V. Bertone, *APFEL++: A new PDF evolution library in C++*, *PoS DIS2017* (2018) 201 [[1708.00911](#)].
- [39] A. Candido, F. Hekhorn and G. Magni, *EKO: evolution kernel operators*, *Eur. Phys. J. C* **82** (2022) 976 [[2202.02338](#)].
- [40] G. P. Salam and J. Rojo, *A Higher Order Perturbative Parton Evolution Toolkit (HOPPET)*, *Comput. Phys. Commun.* **180** (2009) 120 [[0804.3755](#)].
- [41] A. Vogt, *Efficient evolution of unpolarized and polarized parton distributions with QCD-PEGASUS*, *Comput. Phys. Commun.* **170** (2005) 65 [[hep-ph/0408244](#)].
- [42] M. Botje, *QCDNUM: Fast QCD Evolution and Convolution*, *Comput. Phys. Commun.* **182** (2011) 490 [[1005.1481](#)].
- [43] J. McGowan, T. Cridge, L. A. Harland-Lang and R. S. Thorne, *Approximate N^3 LO parton distribution functions with theoretical uncertainties: MSHT20a N^3 LO PDFs*, *Eur. Phys. J. C* **83** (2023) 185 [[2207.04739](#)].

- [44] T. Cridge, L. A. Harland-Lang and R. S. Thorne, *Combining QED and Approximate N^3 LO QCD Corrections in a Global PDF Fit: MSHT20qed_an3lo PDFs*, [2312.07665](#).
- [45] F. Hekhorn and G. Magni, *DGLAP evolution of parton distributions at approximate N^3 LO*, [2306.15294](#).
- [46] NNPDF collaboration, *The Path to N^3 LO Parton Distributions*, [2402.18635](#).
- [47] Y. L. Dokshitzer, G. Marchesini and G. P. Salam, *Revisiting parton evolution and the large- x limit*, *Phys. Lett. B* **634** (2006) 504 [[hep-ph/0511302](#)].
- [48] V. S. Fadin, E. A. Kuraev and L. N. Lipatov, *On the Pomeron Singularity in Asymptotically Free Theories*, *Phys. Lett. B* **60** (1975) 50.
- [49] E. A. Kuraev, L. N. Lipatov and V. S. Fadin, *Multi - Reggeon Processes in the Yang-Mills Theory*, *Sov. Phys. JETP* **44** (1976) 443.
- [50] L. N. Lipatov, *Reggeization of the Vector Meson and the Vacuum Singularity in Nonabelian Gauge Theories*, *Sov. J. Nucl. Phys.* **23** (1976) 338.
- [51] E. A. Kuraev, L. N. Lipatov and V. S. Fadin, *The Pomeron Singularity in Nonabelian Gauge Theories*, *Sov. Phys. JETP* **45** (1977) 199.
- [52] V. S. Fadin and L. N. Lipatov, *BFKL pomeron in the next-to-leading approximation*, *Phys. Lett. B* **429** (1998) 127 [[hep-ph/9802290](#)].
- [53] T. Jaroszewicz, *Gluonic Regge Singularities and Anomalous Dimensions in QCD*, *Phys. Lett. B* **116** (1982) 291.
- [54] M. Ciafaloni and G. Camici, *Energy scale(s) and next-to-leading BFKL equation*, *Phys. Lett. B* **430** (1998) 349 [[hep-ph/9803389](#)].
- [55] S. Catani and F. Hautmann, *High-energy factorization and small x deep inelastic scattering beyond leading order*, *Nucl. Phys. B* **427** (1994) 475 [[hep-ph/9405388](#)].
- [56] T. Cridge, L. A. Harland-Lang and R. S. Thorne, *The impact of LHC jet and Zp_T data at up to approximate N^3 LO order in the MSHT global PDF fit*, *Eur. Phys. J. C* **84** (2024) 446 [[2312.12505](#)].
- [57] T. Cridge, L. A. Harland-Lang and R. S. Thorne, *A first determination of the strong coupling α_S at approximate N^3 LO order in a global PDF fit*, [2404.02964](#).
- [58] A. Barontini, A. Candido, J. M. Cruz-Martinez, F. Hekhorn and C. Schwan, *Pipeline: Industrialization of High-Energy Theory Predictions*, [2302.12124](#).
- [59] J. M. Henn, G. P. Korchemsky and B. Mistlberger, *The full four-loop cusp anomalous dimension in $\mathcal{N} = 4$ super Yang-Mills and QCD*, *JHEP* **04** (2020) 018 [[1911.10174](#)].
- [60] C. Duhr, B. Mistlberger and G. Vita, *Soft integrals and soft anomalous dimensions at N^3 LO and beyond*, *JHEP* **09** (2022) 155 [[2205.04493](#)].
- [61] A. A. Almasy, G. Soar and A. Vogt, *Generalized double-logarithmic large- x resummation in inclusive deep-inelastic scattering*, *JHEP* **03** (2011) 030 [[1012.3352](#)].
- [62] J. Davies, C. H. Kom, S. Moch and A. Vogt, *Resummation of small- x double logarithms in QCD: inclusive deep-inelastic scattering*, *JHEP* **08** (2022) 135 [[2202.10362](#)].
- [63] R. D. Ball and S. Forte, *The Small x behavior of Altarelli-Parisi splitting functions*, *Phys. Lett. B* **465** (1999) 271 [[hep-ph/9906222](#)].
- [64] M. Bonvini and S. Marzani, *Four-loop splitting functions at small x* , *JHEP* **06** (2018) 145 [[1805.06460](#)].

- [65] NNPDF collaboration, *Parton Distributions with Theory Uncertainties: General Formalism and First Phenomenological Studies*, *Eur. Phys. J. C* **79** (2019) 931 [[1906.10698](#)].
- [66] NNPDF collaboration, *Determination of the theory uncertainties from missing higher orders on NNLO parton distributions with percent accuracy*, [2401.10319](#).
- [67] A. von Manteuffel, E. Panzer and R. M. Schabinger, *Cusp and collinear anomalous dimensions in four-loop QCD from form factors*, *Phys. Rev. Lett.* **124** (2020) 162001 [[2002.04617](#)].
- [68] G. Das, S.-O. Moch and A. Vogt, *Soft corrections to inclusive deep-inelastic scattering at four loops and beyond*, *JHEP* **03** (2020) 116 [[1912.12920](#)].
- [69] G. Das, S. Moch and A. Vogt, *Approximate four-loop QCD corrections to the Higgs-boson production cross section*, *Phys. Lett. B* **807** (2020) 135546 [[2004.00563](#)].
- [70] G. Soar, S. Moch, J. A. M. Vermaseren and A. Vogt, *On Higgs-exchange DIS, physical evolution kernels and fourth-order splitting functions at large x*, *Nucl. Phys. B* **832** (2010) 152 [[0912.0369](#)].
- [71] A. Vogt, *Leading logarithmic large-x resummation of off-diagonal splitting functions and coefficient functions*, *Phys. Lett. B* **691** (2010) 77 [[1005.1606](#)].
- [72] M. Ciafaloni and D. Colferai, *Dimensional regularisation and factorisation schemes in the BFKL equation at subleading level*, *JHEP* **09** (2005) 069 [[hep-ph/0507106](#)].
- [73] M. Ciafaloni, D. Colferai, G. P. Salam and A. M. Stasto, *Minimal subtraction vs. physical factorisation schemes in small-x QCD*, *Phys. Lett. B* **635** (2006) 320 [[hep-ph/0601200](#)].
- [74] M. Diehl, R. Nagar and F. J. Tackmann, *ChiliPDF: Chebyshev interpolation for parton distributions*, *Eur. Phys. J. C* **82** (2022) 257 [[2112.09703](#)].
- [75] I. Bierenbaum, J. Blumlein and S. Klein, *Mellin Moments of the $O(\alpha_s^3(s))$ Heavy Flavor Contributions to unpolarized Deep-Inelastic Scattering at $Q^2 \gg m^2$ and Anomalous Dimensions*, *Nucl. Phys. B* **820** (2009) 417 [[0904.3563](#)].
- [76] J. Ablinger, A. Behring, J. Blümlein, A. De Freitas, A. Hasselhuhn, A. von Manteuffel et al., *The 3-Loop Non-Singlet Heavy Flavor Contributions and Anomalous Dimensions for the Structure Function $F_2(x, Q^2)$ and Transversity*, *Nucl. Phys. B* **886** (2014) 733 [[1406.4654](#)].
- [77] J. Blümlein, P. Marquard, C. Schneider and K. Schönwald, *The three-loop unpolarized and polarized non-singlet anomalous dimensions from off shell operator matrix elements*, *Nucl. Phys. B* **971** (2021) 115542 [[2107.06267](#)].
- [78] J. Ablinger, J. Blümlein, A. De Freitas, A. Hasselhuhn, A. von Manteuffel, M. Round et al., *The $O(\alpha_s^3 T_F^2)$ Contributions to the Gluonic Operator Matrix Element*, *Nucl. Phys. B* **885** (2014) 280 [[1405.4259](#)].
- [79] J. Ablinger, J. Blümlein, A. De Freitas, A. Hasselhuhn, A. von Manteuffel, M. Round et al., *3-loop Massive $O(T_F^2)$ Contributions to the DIS Operator Matrix Element A_{gg}* , *Nucl. Part. Phys. Proc.* **258-259** (2015) 37 [[1409.1435](#)].
- [80] J. Ablinger, J. Blümlein, A. De Freitas, A. Hasselhuhn, A. von Manteuffel, M. Round et al., *The transition matrix element $A_{gq}(N)$ of the variable flavor number scheme at $O(\alpha_s^3)$* , *Nuclear Physics B* **882** (2014) 263 [[1402.0359](#)].
- [81] R. S. Thorne, T. Cridge and L. A. Harland-Lang, *Updates of MSHT PDFs (to appear)*, [24xx.xxxxx](#).